



HAL
open science

The Hippo pathway controls myofibril assembly and muscle fiber growth by regulating sarcomeric gene expression

Aynur Kaya-Çopur, Fabio Marchiano, Marco Hein, Daniel Alpern, Julie Russeil, Nuno Miguel Luis, Matthias Mann, Bart Deplancke, Bianca Habermann, Frank Schnorrer

► To cite this version:

Aynur Kaya-Çopur, Fabio Marchiano, Marco Hein, Daniel Alpern, Julie Russeil, et al.. The Hippo pathway controls myofibril assembly and muscle fiber growth by regulating sarcomeric gene expression. 2020. hal-03028020

HAL Id: hal-03028020

<https://hal.science/hal-03028020>

Preprint submitted on 27 Nov 2020

HAL is a multi-disciplinary open access archive for the deposit and dissemination of scientific research documents, whether they are published or not. The documents may come from teaching and research institutions in France or abroad, or from public or private research centers.

L'archive ouverte pluridisciplinaire **HAL**, est destinée au dépôt et à la diffusion de documents scientifiques de niveau recherche, publiés ou non, émanant des établissements d'enseignement et de recherche français ou étrangers, des laboratoires publics ou privés.

1 **The Hippo pathway controls myofibril assembly and muscle fiber growth by**
2 **regulating sarcomeric gene expression**

3

4 Aynur Kaya-Çopur^{1,2}, Fabio Marchiano¹, Marco Y. Hein², Daniel Alpern³, Julie Russeil³,
5 Nuno Miguel Luis¹, Matthias Mann², Bart Deplancke³, Bianca H. Habermann¹, Frank
6 Schnorrer^{1,2}

7

8

9 ¹ Aix Marseille University, CNRS, IBDM, Turing Center for Living Systems, 13288
10 Marseille, France

11 ² Max Planck Institute of Biochemistry, 82152 Martinsried, Germany

12 ³ Institute of Bioengineering, School of Life Sciences, École Polytechnique Fédérale de
13 Lausanne (EPFL), 1015 Lausanne, Switzerland

14

15

16 Correspondence should be addressed to:

17 aynur.kaya-copur@univ-amu.fr

18 frank.schnorrer@univ-amu.fr

19 keywords: muscle; sarcomere; myofibril; Hippo; yorkie; *Drosophila*; growth; Dlg5;

20 STRIPAK

21

22

23 **Abstract**

24 **Skeletal muscles are composed of gigantic cells called muscle fibers, packed with**
25 **force-producing myofibrils. During development the size of individual muscle fibers**
26 **must dramatically enlarge to match with skeletal growth. How muscle growth is**
27 **coordinated with growth of the contractile apparatus is not understood. Here, we**
28 **use the large *Drosophila* flight muscles to mechanistically decipher how muscle fiber**
29 **growth is controlled. We find that regulated activity of core members of the Hippo**
30 **pathway is required to support flight muscle growth. Interestingly, we identify Dlg5**
31 **and Slmap as regulators of the STRIPAK phosphatase, which negatively regulates**
32 **Hippo to enable post-mitotic muscle growth. Mechanistically, we show that the**
33 **Hippo pathway controls timing and levels of sarcomeric gene expression during**
34 **development and thus regulates the key components that physically mediate muscle**
35 **growth. Since Dlg5, STRIPAK and the Hippo pathway are conserved a similar**
36 **mechanism may contribute to muscle or cardiomyocyte growth in humans.**

37

38 **Introduction**

39 Mammalian skeletal muscles are built from gigantic cells called muscle fibers, up to
40 several centimetres long, that mechanically link distant skeletal elements. Muscle forces
41 are produced by highly regular molecular arrays of actin, myosin and titin filaments
42 called sarcomeres. Each sarcomere has a length of about three micrometres in relaxed
43 human skeletal muscles (Ehler and Gautel, 2008; Llewellyn et al., 2008; Regev et al.,
44 2011). Thus, hundreds of sarcomeres need to assemble into long chains called myofibrils
45 in order to generate force across the entire muscle fiber (Lemke and Schnorrer, 2017).
46 Large muscle fibers contain many parallel myofibrils, which are laterally aligned to a
47 cross-striated pattern to effectively power animal locomotion (Gautel, 2008; Schiaffino et
48 al., 2013). How muscle fibers grow to these enormous sizes and how their growth is
49 coordinated with the assembly and growth of the individual myofibrils within the muscle
50 is a challenging biological problem that is not well understood.

51 Muscle fibers are built during animal development. Initially, many small
52 myoblasts fuse to myotubes, whose long-ends then mechanically connect to tendon cells
53 (Kim et al., 2015; Schnorrer and Dickson, 2004). This enables the build-up of mechanical
54 tension within myotubes, which consecutively triggers myofibril assembly and the
55 transition of myotubes to early myofibers (Weitkunat et al., 2017; 2014). Following
56 myofibril assembly, the immature myofibrils mature and build functional sarcomeres. To
57 do so each myofibril grows in length and diameter and thereby supports the extensive
58 muscle fiber growth during embryonic and postembryonic development (González-
59 Morales et al., 2019; Orfanos et al., 2015; Reedy and Beall, 1993; Sanger et al., 2017;
60 Sparrow and Schöck, 2009). For the correct developmental sequence of myofibril

61 morphogenesis, the protein concentrations of the various sarcomeric components need to
62 be precisely regulated (Orfanos and Sparrow, 2013; Schönbauer et al., 2011). This is
63 particularly prominent in mammalian muscle fibers, in which sarcomeric proteins
64 transcriptionally switch isoforms from embryonic to neonatal and finally adult isoforms
65 (Schiaffino, 2018; Schiaffino et al., 2015). In *Drosophila* indirect flight muscles,
66 transcription of sarcomeric protein coding genes starts just before myofibril assembly and
67 is then strongly boosted during myofibril maturation, when myofibrils grow in length and
68 width (González-Morales et al., 2019; Shwartz et al., 2016; Spletter et al., 2018).
69 Concomitantly with the growth of the myofibrils, also the mitochondria grow in size
70 (Avellaneda et al., 2020). How this precise transcriptional control is achieved and
71 coordinated with muscle fiber growth is unclear.

72 One central pathway controlling organ size during development and
73 tumorigenesis is the Hippo pathway, which regulates the activity of the growth promoting
74 transcriptional coactivator Yorkie (Yki, YAP and TAZ in mammals) (Pan, 2010;
75 Zanconato et al., 2019). The core of the pathway is composed of a kinase cascade with
76 Hippo (Hpo; Mst1 and Mst2 in mammals) phosphorylating the downstream kinase Warts
77 (Wts; Lats1 and Lats2 in mammals) (Udan et al., 2003; Wu et al., 2003). Phosphorylated
78 Wts is active and in turn phosphorylates Yki (Huang et al., 2005), leading to the
79 cytoplasmic retention of Phospho-Yki by 14-3-3 proteins (Dong et al., 2007; Oh and
80 Irvine, 2008; Ren et al., 2010). When the pathway is not active unphosphorylated Yki
81 enters into the nucleus, binds to the TEAD protein Scalloped (Sd) and turns on
82 transcriptional targets (Goulev et al., 2008; Wu et al., 2008; Zhang et al., 2008). The
83 majority of these targets promote organ growth by suppressing apoptosis and stimulating

84 cell growth and cell proliferation (Harvey and Tapon, 2007).

85 A key control step of the Hippo pathway is the localisation and kinase activity of
86 Hippo. In epithelial cells, the scaffold protein Salvador promotes Hippo kinase activity by
87 localising Hippo to the plasma membrane (Yin et al., 2013) and by inhibiting a large
88 protein complex called the STRIPAK (Striatin-interacting phosphatase and kinase)
89 complex (Bae et al., 2017). The STRIPAK complex contains PP2A as active phosphatase,
90 which dephosphorylates a key Hippo auto-phosphorylation site and thus inhibits Hippo
91 activity (Ribeiro et al., 2010; Zheng et al., 2017). dRassf can promote this recruitment of
92 STRIPAK to Hippo and thus inactivate Hippo (Polesello et al., 2006; Ribeiro et al., 2010).
93 Furthermore, the Hippo pathway can also be regulated downstream by membrane
94 localisation of the kinase Warts by Merlin binding, which promotes Warts
95 phosphorylation by Hippo and thus activation of the pathway (Yin et al., 2013). Finally,
96 mechanical stretch of the epithelial cell cortex was shown to directly inhibit the Hippo
97 pathway, likely mediated by the spectrin network at the cortex, promoting nuclear
98 localisation of Yorkie (Fletcher et al., 2018; 2015). Despite this detailed knowledge about
99 Hippo regulation in proliferating epithelial cells, little is known about how the Hippo
100 pathway is regulated during post-mitotic muscle development and how it impacts muscle
101 growth.

102 Here, we employ a systematic *in vivo* muscle-specific RNAi screen and identify
103 various components of the Hippo pathway as essential post-mitotic regulators of flight
104 muscle morphogenesis. We find that loss of Dlg5 or of the STRIPAK complex member
105 Slmap, which interacts with Dlg5, as well as loss of the transcriptional regulator Yorkie
106 results in too small muscles. These small muscles express lower levels of sarcomeric

107 proteins and as a consequence contain fewer and defective myofibrils. Conversely, over-
108 activation of Yorkie, either by removing the negative regulators Hippo or Warts or by
109 enabling constitutive nuclear entry of Yorkie results in premature and excessive
110 expression of sarcomeric proteins and consequently in chaotic myofibril assembly.
111 Therefore, our findings suggest that the Hippo pathway contributes to the precise timing
112 of sarcomeric gene expression and thus can generate a feedback mechanism for muscles
113 to precisely coordinate sarcomeric protein levels during myofibril assembly and myofibril
114 maturation. This provides an attractive mechanism for how regulated transcription can
115 coordinate muscle growth with myofibril morphogenesis.

116

117

118

119

120 **Results**

121 **Growth of *Drosophila* flight muscles**

122 We chose the *Drosophila* indirect flight muscles to investigate post-mitotic muscle fiber
123 growth. These muscles consist of two groups, the dorsal-longitudinal flight muscles
124 (DLMs) and the dorso-ventral flight muscles (DVMs). Both groups form in the second
125 thoracic segment during pupal development and despite differences during myoblast
126 fusion and myotube attachment determining their location in the thorax, their
127 development after 24 h after puparium formation (APF) is very similar (Dutta et al.,
128 2004; Fernandes et al., 1991; Schönbauer et al., 2011). Thus, we focused our studies on
129 the DLMs and for simplicity call them flight muscles in the remainder of the manuscript.

130 In order to quantify muscle fiber growth we measured fiber length and cross-
131 sectional area of wild-type DLM flight muscles. At 24 h APF (at 27 °C) myoblast fusion
132 is largely finished (Weitkunat et al., 2014), and the fibers have a length of about 270 μm
133 and a cross-sectional area of about 1000 μm^2 (Figure 1A,C, Supplementary Table 1).
134 Then, flight muscles build up mechanical tension, compact to about 220 μm in length,
135 while their diameter grows to about 2000 μm^2 , and assemble the immature myofibrils at
136 32 h APF (Lemke et al., 2019; Weitkunat et al., 2014) (Figure 1A,C). After 32 h, flight
137 muscles grow about 2.5 times in length while keeping the same diameter until 48 h APF.
138 After 48 h APF, they grow further to about 800 μm in length while increasing in diameter
139 to almost 4000 μm^2 until 90 h APF, which is shortly before eclosion at 27 °C (Figure 1A,
140 Supplementary Table 1) (Spletter et al., 2018). Thus, in total, the volume of the
141 individual muscle fibers increases more than 10-fold in less than 3 days (Figure 1A,
142 Supplementary Table 1). Thus, indirect flight muscles are a good model to study rapid

143 post-mitotic muscle fiber growth.

144

145 ***Dlg5* and *Slmap* are essential for flight muscle morphogenesis**

146 To identify regulators of muscle growth we have investigated genes identified in a
147 genome-wide muscle-specific RNAi study that had resulted in flightless or late
148 developmental lethality when knocked-down using muscle-specific *Mef2*-GAL4
149 (Schnorrer et al., 2010). Our analysis identified two genes *Dlg5* (*Discs large 5*, *CG6509*)
150 and *Slmap* (*Sarcolemma associated protein*, *CG17494*), which are conserved from
151 *Drosophila* to human and when knocked-down using several independent RNAi
152 constructs result in viable but completely flightless flies (Figure 1 supplement 1,
153 Supplementary Table 1). Inspection of the thoraces of these animals revealed complete
154 flight muscle atrophy in pupae at 90 h APF (Figure 1B). Expression of a UAS-*Dlg5*-GFP
155 but not a UAS-GFP-Gma control construct, was able to rescue the number of muscle
156 fibers of *Dlg5* knock-down (*Dlg5-IR-1*) flies to wild type providing further strong
157 evidence for the specificity of the knock-down phenotype (Figure 1D). We conclude that
158 *Dlg5* and *Slmap* are two conserved genes essential for flight muscle morphogenesis
159 during pupal stages.

160 To identify the developmental time point when *Dlg5* and *Slmap* are required, we
161 analysed pupal stages and found that at 24 h APF all flight muscles are present after *Dlg5*
162 or *Slmap* knockdown. However, the fibers are more than 20% longer than wild type and
163 fail to compact at 32 h APF when myofibrils normally assemble (Figure 1B,C,
164 Supplementary Table 1). Interestingly, after 32 h APF, when wild-type myofibers
165 strongly grow in length, *Dlg5* and *Slmap* knock-down fibers undergo complete flight

166 muscle atrophy until 48 h APF (Figure 1B). Taken together, these data demonstrate that
167 *Dlg5* and *Slmap* play an essential role during stages of myofibril assembly and muscle
168 fiber growth.

169

170 ***Dlg5* interacts with *Slmap*, a STRIPAK complex member, in *Drosophila* muscle**

171 To define a molecular mechanism for how *Dlg5* regulates muscle morphogenesis we
172 performed GFP immunoprecipitation followed by mass-spectrometry, using the
173 functional *UAS-Dlg5-GFP*, which was expressed in pupal muscles with *Mef2-GAL4*.
174 Interestingly, we not only identified *Slmap* as a binding partner of *Dlg5* in muscle, but
175 also *Fgop2*, *GckIII*, *Striatin (Cka)*, and the catalytic subunit of PP2A phosphatase (*Mts*)
176 (Figure 2A,B, Supplementary Table 1). All these proteins are members of the STRIPAK
177 complex and have been described to interact closely in mammals (Hwang and Pallas,
178 2014). This suggests that the composition of the STRIPAK complex in fly muscles is
179 similar to mammals (Figure 2C), and *Dlg5* is either a core member or closely interacts
180 with this complex in muscle.

181 To functionally test if members of the STRIPAK complex other than *Dlg5* and
182 *Slmap* play a similarly important role in flight muscles, we knocked-down various
183 component members and found that knock-down of *Striatin (Cka)* and *Strip* indeed result
184 in very similar phenotypes to *Dlg5* and *Slmap* knock-down: flight muscles at 32 h APF
185 are longer than wild type, suggesting a fiber compaction defect, and undergo muscle
186 atrophy after 32 h APF (Figure 2D,E). Together, these data show that *Dlg5* interacts with
187 the STRIPAK complex in flight muscles, of which several members including *Slmap* are
188 important for flight muscle morphogenesis.

189

190 **The Hippo pathway regulates the developmental timing of muscle morphogenesis**

191 As the STRIPAK complex was shown to dephosphorylate and thus inactivate Hippo
192 (Ribeiro et al., 2010; Zheng et al., 2017), we wondered if the muscle morphogenesis
193 phenotype we observed could be linked to a function of the Hippo pathway in growing
194 flight muscles. When knocking-down the Hippo pathway transcriptional co-activator
195 *yorkie* in muscles, we observed a failure of muscle compaction at 32 h APF, flight muscle
196 atrophy at 48 h APF and consequently flightless adults (Figure 3A,B, Figure 3
197 supplement 1A, Supplementary Table 1). The myofiber compaction defect of *yorkie*
198 knock-down muscles is corroborated by fiber cross-sections at 24 h and 32 h APF
199 revealing much thinner muscles and phenocopying the *Dlg5* and *Slmap* loss of function
200 (Figure 3 supplement 1B).

201 In contrast to the myofiber compaction defect of *yorkie* knock-down muscles,
202 expression of an activated form of Yorkie (*yorkie-CA*), which cannot be phosphorylated
203 by Warts, results in premature muscle fiber compaction already at 24 h APF and strongly
204 hyper-compacted muscle fibers at 32 h APF (Figure 3A,B). The increased cross-sectional
205 area is particularly obvious in cross-sections of *yorkie-CA* fibers (Figure 3 supplement
206 1B). Importantly, we observed the same phenotypes after knock-down of each of the two
207 kinases *hippo* and *warts*, both negative regulators of Yorkie nuclear entry (Figure 3A,B).
208 This strongly suggests that the Hippo pathway, by regulating phosphorylation of the
209 transcriptional co-activator Yorkie, is essential for the correct developmental timing of
210 flight muscle morphogenesis: too much active Yorkie accelerates myofiber compaction,
211 while too little active Yorkie blocks it.

212 To further corroborate that the STRIPAK complex regulates the Hippo pathway in
213 flight muscles we used a recently characterised Hippo construct (*hippo[4A/431T]*), which
214 lacks the four auto-phosphorylation sites in Hippo required to bind to the STRIPAK
215 phosphatase complex via Slmap. This Hippo[4A/431T] protein cannot be
216 dephosphorylated on regulatory T195 by STRIPAK and thus is constitutively active
217 (Zheng et al., 2017). Interestingly, expression of *hippo[4A/431T]* in muscle after *Mef2-*
218 *GAL4* driven flip-out also resulted in a muscle fiber compaction defect at 32 h APF and
219 muscle atrophy thereafter, phenocopying the STRIPAK and *yorkie* loss of function
220 phenotypes (Figure 3C). Taken all these data together, we conclude that Dlg5 and
221 members of the STRIPAK complex are key regulators of the Hippo pathway, which
222 controls the developmental timing of flight muscle morphogenesis in *Drosophila*.

223

224 **The Hippo pathway is required post-mitotically in flight muscle fibers**

225 Indirect flight muscles are formed by fusion of several hundred myoblasts until 24 h APF
226 (Weitkunat et al., 2014). These myoblasts emerge during embryonic development and
227 proliferate extensively during larval stages (Bate et al., 1991; Gunage et al., 2014; Roy
228 and VijayRaghavan, 1998). As knock-down of *Dlg5*, STRIPAK complex and Hippo
229 pathway members with *Mef2-GAL4* results in flightlessness and not in lethality (except
230 for *warts*, see Figure 3 - supplement 1), it is unlikely that general myoblast proliferation
231 during larval stages is affected, which would result in defects of all adult muscles.
232 However, since *Mef2-GAL4* is already active during larval stages, we wanted to exclude
233 that the observed muscle phenotypes are caused by myoblasts proliferation defects during
234 larval stages. Hence, we conditionally activated GAL4 only during pupal stages using

235 temperature sensitive GAL80 (GAL80ts, see Methods)(McGuire et al., 2003) and
236 quantified myoblast fusion rates by counting the nuclei of dorsal longitudinal flight
237 muscle 4 (DLM4). We found comparable numbers of nuclei at 24 h APF ruling out a
238 major contribution of myoblast proliferation or fusion to the phenotype (Figure 4
239 supplement 1).

240 Importantly, these GAL80ts *Mef2-GAL4 Dlg5* and *yorkie* knock-down muscles do
241 display the same fiber compaction defect as observed with *Mef2-GAL4* resulting in
242 longer but thinner fibers with grossly comparable volumes at 24 h APF (*yorkie-IR* is
243 slightly smaller) (Figure 4A,B). These fibers do not compact at 32 h APF and undergo
244 atrophy leading to no remaining fibers at 48 h or 90 h APF (Figure 4C, D), phenocopying
245 the constitutive knock-down of *Dlg5* or *yorkie*. Conversely, conditional expression of
246 *yorkie-CA* during pupal stages results in premature compaction at 24 h APF and very
247 short fibers at 32 h APF that grow to disorganised fibers at 90 h APF (Figure 4A-D).
248 These phenotypes resemble the constitutive *Mef2-GAL4* driven phenotypes
249 demonstrating a role for *Dlg5* and *yorkie* in muscle fibers during pupal stages.

250 To further corroborate a post-mitotic role of the Hippo pathway in muscle fibers,
251 we over-expressed *hippo* with the strong, strictly post-mitotic flight muscle specific
252 driver *Act88F-GAL4*, which is only active after myoblast fusion (Bryantsev et al., 2012;
253 Spletter et al., 2018). This post-mitotic over-expression of *hippo* resulted in flight muscle
254 compaction defects at 32 h APF and muscle atrophy at 48 h APF (Figure 4E). Together,
255 these data demonstrate that the Hippo pathway and its regulator *Dlg5* are required post-
256 mitotically in flight muscle fibers for the correct timing of morphogenesis.

257

258 **The Hippo pathway regulates post-mitotic muscle fiber growth**

259 The wild-type flight muscle fibers grow in volume from 24 h to 48 APF (see Figure 1),
260 while *yorkie* or *Dlg5* knock-down fibers undergo atrophy after 32 h APF. As the Yorkie
261 activity is known to suppress apoptosis in epithelial tissues (Harvey and Tapon, 2007) we
262 asked if we could rescue fiber atrophy by over-expressing the apoptosis inhibitor Diap1.
263 Indeed, over-expression of Diap1 during pupal stages in GAL80ts *Mef2*-GAL4 (hereafter
264 abbreviated as GAL80ts) *yorkie* and *Dlg5* knock-down fibers substantially rescues fiber
265 atrophy, often resulting in the normal number of six muscle fibers at 48 h APF (Figure
266 5A, compare to Figure 4C). This demonstrates that apoptosis contributes to flight muscle
267 fiber atrophy in *yorkie* and *Dlg5* knock-down muscles.

268 Presence of muscle fibers at 48 h APF enabled us to quantitatively investigate the
269 role of the Hippo pathway during the post-mitotic muscle fiber growth. As in Figure 4,
270 we used digital cross-sections of large confocal stacks to quantify the cross-sectional area
271 of dorsal longitudinal flight muscle 4 (DLM4) and together with the fiber length
272 calculated the fiber volume (Figure 5). Similar to what we showed in Figure 4, GAL80ts
273 *Diap1* expressing control fibers have a comparable volume to GAL80ts *Diap1* expressing
274 *yorkie* and *Dlg5* knock-down fibers at 24 h APF (Figure 5A-C), showing that they start
275 into the muscle growth phase with comparable sizes.

276 However, until 32 h APF, *Diap1* control muscles increase their cross-sectional
277 area followed by growth in length until 48 h APF to increase their volume about 4-fold
278 within 24 h (Figure 5A-C). Interestingly, GAL80ts *Diap1* expressing *yorkie* or *Dlg5*
279 knock-down muscles fail to normally increase their cross-sectional area at 32 h and 48 h
280 APF, thus resulting in smaller volumes at 48 h APF (Figure 5A-C). These thin muscles

281 do not survive until 90 h APF despite over-expression of the apoptosis inhibitor Diap1
282 (Figure 5A). Taken together, these data provide strong evidence that the Hippo pathway
283 and its transcriptional co-activator Yorkie are required to enable normal post-mitotic
284 growth of flight muscle fibers, likely by regulating the developmental timing of muscle
285 morphogenesis.

286

287 **The Hippo pathway is essential for myofibrillogenesis**

288 To investigate the molecular mechanism of the muscle growth defect in detail, we
289 quantified myofibrillogenesis in these muscles. Control *Diap1* expressing muscles have
290 assembled immature myofibrils at 32 h APF (Weitkunat et al., 2014). These immature
291 myofibrils are continuous and thus can be easily traced throughout the entire field of view
292 (Figure 6A,B, Figure 6 supplement 1A). In contrast, GAL80ts *Diap1* expressing *yorkie*
293 and *Dlg5* knock-down muscles fail to properly assemble their myofibrils at 32 h APF
294 resulting in only short myofibril traces (Figure 6A,B, Figure 6 supplement 1A).
295 Concomitant with the myofibril assembly defect, we also found that the spacing of the
296 nuclei is defective. In control muscle fibers the nuclei are present mainly as single rows
297 located between myofibril bundles, whereas in *yorkie* and *Dlg5* knock-down muscles
298 they form large centrally located clusters (Figure 6 supplement 1B). This indicates that at
299 32 h APF, Hippo signalling is required within the muscle fibers to trigger proper
300 myofibril assembly and nuclear positioning.

301 The myofibril defect becomes even more pronounced at 48 h APF when control
302 myofibrils have matured and sarcomeres are easily discernable (Figure 6A), while no
303 organised sarcomeres are present in GAL80ts *yorkie* and *Dlg5* knock-down muscles and

304 myofibril traces remain short (Figure 6A,B, Figure 6 supplement 1A). Furthermore, cryo
305 cross-sections revealed that not only the cross-sectional area but also the total number of
306 myofibrils is strongly reduced in GAL80ts *yorkie* and *Dlg5* knock-down muscles
307 compared to control (Figure 6C,D, Figure 6 supplement 1C). These data demonstrate that
308 the Hippo pathway controls both the morphological quality of the myofibrils at the
309 assembly and maturation stages as well as their quantity. As myofibrils occupy most of
310 the muscle fiber space, their reduced amount likely causes the reduced muscle size in
311 *Dlg5* or *yorkie* knock-down fibers.

312

313 **Yorkie is a transcriptional co-regulator in muscle fibers**

314 It was recently shown that the transcription of most sarcomere key components is tightly
315 regulated starting shortly before myofibril assembly and being strongly boosted during
316 myofibril maturation (Spletter et al., 2018). Thus, we reasoned that Yorkie activity may
317 be involved in this transcriptional regulation step to control the timing of
318 myofibrillogenesis. However, it had also been recently shown that Yorkie can regulate
319 myosin contractility directly at the cell membrane without entering into the nucleus (Xu
320 et al., 2018). As we have thus far failed to unambiguously locate Yorkie protein in
321 muscle fibers during development, we used genetic tools to address this important point.
322 To test whether Yorkie may play a role outside of the nucleus, we manipulated Yorkie
323 levels by over-expressing different Yorkie variants post-mitotically using *Act88F*-GAL4
324 and investigated the consequences at 24 h and 32 h APF. Over-expression of either
325 Yorkie-CA, whose import into the nucleus is uncoupled from the Hippo pathway, or
326 wild-type Yorkie, whose nuclear import is regulated by Hippo, both result in premature

327 muscle fiber compaction at 24 h APF, with seemingly normal actin filaments (Figure 6E).
328 Strikingly, the muscle fiber hyper-compaction at 32 h APF coincides with a chaotic
329 organisation of the myofibrils, with many myofibrils not running in parallel but in various
330 directions (Figure 6E, Figure 6 supplement 1D). This suggests that the hyper-compaction
331 phenotype upon Yorkie over-expression is likely caused by uncontrolled and premature
332 force production of the chaotically assembling myofibrils.

333 In contrast, over-expression of a membrane-anchored myristoylated form of
334 Yorkie, which has been shown to activate myosin contractility at the epithelial cell cortex
335 without going into the nucleus (Xu et al., 2018), does not result in premature muscle fiber
336 compaction at 24 h APF. Furthermore, these muscles display normally oriented parallel
337 myofibrils at 32h APF (Figure 6E). These results indicate that the observed myofibril and
338 fiber compaction defects are caused by a transcriptional response of Yorkie in the nucleus.

339 This interpretation is corroborated by loss of function data of the transcriptional
340 activator *scalloped* (*sd*), which is the essential transcriptional co-factor of Yorkie in the
341 nucleus. Knock-down of *scalloped* results in severe muscle atrophy and no remaining
342 muscles at 90 h APF (Figure 6 supplement 1E). Together, these genetic data suggest that
343 Hippo signalling regulates Yorkie phosphorylation and thus its nuclear entry to trigger a
344 transcriptional response that controls myofibril development and muscle fiber growth.

345

346 **The Hippo pathway controls expression of key sarcomere components**

347 To investigate the transcriptional role of the Hippo pathway during flight muscle
348 development we performed muscle-specific transcriptomics of wild-type flight muscles
349 compared to different *yorkie* ‘loss of function’ (*Dlg5-IR*, *Slmap-IR* and *yorkie-IR*) and

350 *yorkie* ‘gain of function’ (*yorkie-CA* and *hippo-IR*) conditions. We dissected flight
351 muscles from 24 h and 32 h APF, isolated RNA and applied a sensitive 3-prime end
352 mRNA sequencing method (BRB-seq)(Alpern et al., 2019), which handles small amounts
353 of mRNA (see Methods). We found a clustering of biological replicates and similar
354 genotypes using principle components analysis and comparable read count distributions
355 across all samples (Figure 7 supplement 1). This verifies BRB-seq as a reliable method to
356 quantitatively compare gene expression from small amounts of developing muscle tissue
357 across multiple samples.

358 We applied the selection criteria $\log_2FC > 1$ and adjusted p-value < 0.05 to
359 identify differentially expressed genes compared to wild type (Supplementary Table 2).
360 Applying FlyEnrichr (Kuleshov et al., 2016) on the differential data sets, we found a
361 strong enrichment for muscle and, in particular, for sarcomere and myofibril Gene
362 Ontology terms (GO-terms) in the differentially expressed genes of all three *yorkie* ‘loss
363 of function’ muscle genotypes (*Dlg5-IR*, *Slmap-IR* and *yorkie-IR*) at 24 h APF (Figure
364 7A, Supplementary Table 3). Importantly, expression of many core sarcomeric
365 components, including both titin homologs *sallimus* (*sls*) and *bent* (*bt*), *Myosin heavy*
366 *chain* (*Mhc*), *Myofilin* (*Mf*), *Paramyosin* (*Prm*), tropomyosins (*Tm1*, *Tm2*), flight muscle
367 specific actin (*Act88F*) and *Obscurin* (*Unc-89*), as well as sarcomere dynamics regulators,
368 including myosin phosphatase (*Mbs*), a flight muscle formin (*Fhos*) and the spektraplaklin
369 *shortstop* (*shot*) are consistently reduced in *yorkie* ‘loss of function’ muscle genotypes at
370 24 h APF (Figure 7B). Furthermore, expression of mRNAs coding for proteins linking
371 the nuclei to the cytoskeleton, such as the Nesprin family members *klar* and *Msp300*, are
372 also strongly reduced (Figure 7B), which may explain the observed nuclei position defect

373 in *yorkie* and *Dlg5* knock-down muscles (Figure 6 supplement 1B). *Msp300* and *Prm* are
374 amongst the only 6 genes that are significantly down-regulated in all three loss of
375 function conditions at 24 h APF (Supplementary Table 2). This strongly suggests that
376 nuclear entry of Yorkie contributes to the transcriptional induction of sarcomeric protein
377 coding genes as well as genes important to link the nuclei to the sarcomeres. This
378 transcriptional induction was shown to precede sarcomere assembly (Spletter et al., 2018)
379 and thus may provide a molecular explanation of the observed flight muscle compaction
380 and myofibril assembly defects of *Dlg5-IR*, *Slmap-IR* and *yorkie-IR* muscles.

381 To complement the *yorkie* loss of function conditions, we also performed BRB-
382 seq transcriptomics comparing *yorkie* ‘gain of function’ conditions (*yorkie-CA* and
383 *hippo-IR*) to control. While we found few significantly differentially expressed genes at
384 24 h APF (including an induction of the transcriptional co-regulator *scalloped*)
385 (Supplementary Table 2), we identified many significant changes in mRNA expression in
386 *yorkie-CA* and *hippo-IR* myofibers at 32 h APF (Supplementary Table 2). Strikingly,
387 sarcomeric core components and their regulators are amongst the top up-regulated genes
388 on both lists (Figure 7B, Supplementary Table 2). Consequently, GO-term analysis of the
389 differentially expressed genes identified a strong enrichment for sarcomere and myofibril
390 GO-terms (Figure 7A, Supplementary Table 3). In addition to sarcomeric genes, genes
391 important for myofibril attachment at muscle-tendon junctions, including the integrin
392 attachment complex members *kon*, *if*, *CAP*, *by* and *Kank* are up-regulated in both gain of
393 function genotypes (Figure 7B). Furthermore, we found an up-regulation of Hippo
394 signalling regulators *mask*, which is required for efficient nuclear import of Yki (Sidor et
395 al., 2019), and of the negative regulator *wts* (Figure 7B). This demonstrates that regulated

396 Hippo activity is required to control Yorkie in order to tune expression of mRNAs coding
397 for sarcomeric and myofibril attachment proteins.

398 During the stage of myofibril assembly, the mitochondria morphology changes
399 and the expression of mitochondrial genes increase (Avellaneda et al., 2020; Spletter et
400 al., 2018). Consistently, we found an induction of mitochondria dynamics and protein
401 import regulators (Opa1, Tom40) in *hippo-IR and yorkie-CA* myofibers at 32 h APF as
402 well as a consistent up-regulation of mRNAs coding for respiratory chain components,
403 including the F1F0 ATP synthase complex (complex V) subunit *blw*, the NADH
404 dehydrogenase (ubiquinone) subunit *ND-75* and the Ubiquinol-cytochrome c reductase
405 subunit *UQCR-C2*, which are all required to boost ATP production during muscle fiber
406 growth (Figure 7A,B, Supplementary Table 2). Taken together, these data strongly
407 suggest that the Hippo pathway regulates the correct expression dynamics of many key
408 muscle components, most prominently mRNAs coding for core sarcomeric and
409 mitochondrial proteins to enable myofibril assembly and mitochondrial maturation.

410

411 **Yorkie controls sarcomeric protein dynamics**

412 The most prominent phenotypes of the *yorkie* ‘loss of function’ group (*Dlg5-IR, Slmap-*
413 *IR and yorkie-IR*) are defective muscle fiber compaction and severe myofibril assembly
414 defects at 32 h APF. As the core sarcomeric proteins actin and myosin are required to
415 assemble myofibrils and build up mechanical tension (Loison et al., 2018; Weitkunat et
416 al., 2014) we chose to quantify protein levels of the major actin isoform in flight muscles
417 Actin88F (Act88F) as well as the only *Drosophila* muscle Myosin heavy chain (Mhc).
418 For both, we used GFP fusion proteins expressed under endogenous control (Sarov et al.,

419 2016) and thus avoiding the variations often seen in antibody stainings (see Methods).
420 Consistent with the transcriptomics data, we found a mild reduction of Mhc and Act88F
421 protein levels in *yorkie* knock-down muscles at 24 h APF, which became more
422 pronounced at 32 h APF (Figure 8A-C). This is consistent with the myofibril assembly
423 defects found in *yorkie* knock-down muscles at 32 h APF.

424 Surprisingly, constitutive activation of *yorkie* (*yorkie-CA*) results in a boost of
425 Mhc-GFP and Act88F-GFP protein expression already at 24 h APF, which is maintained
426 at 32 h APF (Figure 8A-C). This increased acto-myosin expression may provide the
427 molecular explanation of the premature compaction phenotype seen in *yorkie-CA* muscles
428 at 24 h APF. Despite being expressed at high levels already at 24 h APF, both proteins
429 fail to prematurely assemble into periodic myofibrils in *yorkie-CA* (Fig. 8A,B).
430 Furthermore, the myofibrils present in *yorkie-CA* at 32 h APF are less regularly organised
431 compared to control, with actin showing less pronounced periodicity (Figure 6
432 supplement 1D). These ectopic localisation patterns of actin and myosin may explain
433 muscle hyper-compaction at 32 h APF and the chaotic arrangement of myofibrils in
434 *yorkie-CA* 90 h APF (see Figure 5C). Taken together, these data provide strong evidence
435 that the Hippo pathway and its transcriptional regulator Yorkie contribute to the timing of
436 myofibril assembly by regulating correct timing and levels of sarcomeric protein
437 expression.

438

439

440

441

442 **Discussion**

443 **The Hippo pathway and post-mitotic muscle fiber growth**

444 Muscle fibers are often enormously large cells, which are densely packed with force
445 producing contractile filaments and ATP producing mitochondria (Willingham et al.,
446 2020). Thus, it appears logical that myofibril and mitochondria content primarily
447 contribute to the size of an individual muscle fiber. To explore the link between
448 myofibrillogenesis and muscle fiber growth, we used the largest *Drosophila* muscle cells,
449 the indirect flight muscles, which are formed by fusion of several hundred myoblasts per
450 muscle fiber and grow more than 10 times in volume after fusion within 72 hours. We
451 provide strong genetic evidence that the regulation of Yorkie nuclear activity by the
452 Hippo pathway is essential to allow post-mitotic flight muscle growth. Loss of function
453 of Yorkie or one of the upstream STRIPAK complex members *Slmap*, *Strip* and *Cka*, as
454 well as *Dlg5*, that regulate Hippo activity, all show the same phenotype: muscle atrophy
455 during the post-mitotic muscle growth phase. Atrophy can be partially suppressed by
456 over-expression of the apoptosis inhibitor *DIAP1*, which then results in small flight
457 muscle fibers, emphasizing the essential role of Yorkie in promoting flight muscle
458 growth.

459 How general is this role of Yorkie and the Hippo pathway in muscle fiber growth?
460 Interestingly, muscle specific loss (*Dlg5-IR*, *Slmap-IR* and *yorkie-IR*) and gain of
461 function of Yorkie (*hippo-IR*, *yorkie-CA*) results in viable but flightless animals. This
462 suggests that the larval muscles and the other adult *Drosophila* muscle fibers such as leg
463 and abdominal muscles can form and function normally in the absence of Yorkie and the
464 Hippo pathway. One reason might be their slower growth rates and their more limited

465 sizes compared to indirect flight muscles. A second reason may relate to the particular
466 myofibrillogenesis mechanism in flight muscles. Flight muscles display individual
467 distinct myofibrils, which all form simultaneously at about 32 h APF (Weitkunat et al.,
468 2014) and then grow in length and diameter to match the volume increase of the muscle
469 fiber (Spletter et al., 2018).

470 The closest mammalian homolog to insect flight muscles is the mammalian heart.
471 Similar to flight muscles, the heart is a very stiff muscle using a stretch-modulated
472 contraction mechanism (Shiels and White, 2008). After birth, mammalian
473 cardiomyocytes stop dividing and all organ growth is achieved post-mitotically by size
474 increase of the individual contractile cells. Interestingly, it was shown that mammalian
475 YAP1 can promote cardiomyocyte survival and growth, as post-mitotic deletion of YAP1
476 results in increased fibrosis and cardiomyocyte apoptosis (Del Re et al., 2013). However,
477 a role for the Hippo pathway in mammalian muscle is not limited to the heart.
478 Constitutive expression of active YAP in adult mouse muscle fibers induces muscle fiber
479 atrophy and deterioration of muscle function (Judson et al., 2013). Furthermore, it has
480 been shown that the mammalian Hippo homolog Mst1 is a key regulator in fast skeletal
481 muscle atrophy (Wei et al., 2013), and more importantly YAP promotes muscle fiber
482 growth by its transcriptional activity requiring TEAD cofactors (Watt et al., 2015). This
483 suggests that the Hippo pathway via its transcriptional regulators Yorkie/YAP/TAZ is a
484 general regulator of muscle fiber growth and survival in animals.

485

486 **Yorkie targets**

487 How does Yorkie mediate flight muscle growth? Our transcriptomics analysis revealed
488 that mRNAs coding for sarcomeric and mitochondrial components are major
489 transcriptional targets of Yorkie in flight muscle. In flies and mammals,
490 Yorkie/YAP/TAZ require transcriptional cofactors of the Tead family (TEA domain
491 containing) to bind to DNA. Interestingly, it has been shown that mammalian homologs
492 Tead1-4 bind to a DNA motif called ‘muscle CAT’ (MCAT), a motif well-known to
493 regulate cardiac skeletal sarcomeric protein expression, including cardiac Troponin T or
494 cardiac actin (Carson et al., 1996; Farrance and Ordahl, 1996; Farrance et al., 1992;
495 Wackerhage et al., 2014). The only *Drosophila* TEAD family member Scalloped binds to
496 a very similar MCAT motif (Wu et al., 2008) and we found loss of *scalloped* shows the
497 same phenotype as loss of function of *yorkie*. This strongly suggests that Yorkie and
498 Scalloped cooperate in *Drosophila* muscle to transcriptionally boost sarcomeric gene
499 expression to enable myofibril assembly and successively flight muscle fiber growth.

500 It has been shown that flight muscle fate is determined by the zinc finger
501 transcriptional regulator Spalt major (Schönbauer et al., 2011). This includes the
502 regulation of all flight muscle-specific sarcomeric components. How Yorkie cooperates
503 with Spalt is to date an open question. One interesting link is that Yorkie and the Hippo
504 pathway are required for the normal expression of *bruno1* (*bru1*, see Figure 7B). Bruno is
505 the major splice regulator of flight muscle alternative splicing of sarcomeric proteins,
506 downstream of Spalt (Spletter et al., 2015). Additionally, Bruno was shown to bind to 3’-
507 UTRs of mRNA to regulate their translation efficiencies (Webster et al., 1997). Another
508 RNA binding protein that requires the Hippo pathway for normal expression is Imp (IGF-
509 II mRNA-binding protein, see Figure 7B). Imp has been shown to regulate the stability

510 and translation of a number of F-actin regulators (Medioni et al., 2014), suggesting that
511 post-transcriptional effects of Hippo signalling can play an important role, too. This may
512 explain the strong up-regulation of Mhc and Act88F proteins levels in *yorkie-CA* muscle
513 at 24 h APF despite little changes at the mRNA level. A similar cross talk between the
514 Hippo pathway and translational regulation via the mTORC1 complex has been
515 suggested in mammals (Hansen et al., 2015).

516

517 **Regulation of the Hippo pathway**

518 How is the Hippo pathway regulated to induce sarcomeric protein expression at the
519 correct time during muscle development? Salvador, Expanded, Merlin and Kibra, which
520 regulate activity or plasma membrane localisation of Hippo in epithelial cells, all appear
521 not to be required in flight muscles (Schnorrer et al., 2010)(and data not shown).
522 However, we find that the core members of the STRIPAK complex Slmap, Strip and Cka
523 as well as Dlg5 are required to regulate Hippo in muscle. Interestingly, Strip and Cka
524 have been shown to bind to each other and regulate either Hippo or other signalling
525 pathways in other *Drosophila* tissues including eye, testis or motor neurons (La Marca et
526 al., 2019; Neal et al., 2020; Neisch et al., 2017). Slmap appears to be the specific adaptor
527 to link STRIPAK to Hippo in muscle (our work) and epithelia in flies (Neal et al., 2020;
528 Zheng et al., 2017) as well as in mammalian cell culture (Bae et al., 2017; Kwan et al.,
529 2016). As Slmap has a single transmembrane domain, it is likely localised to the plasma
530 membrane or t-tubules, membrane invaginations that form during myofibrillogenesis and
531 link the plasma membrane to the forming sarcomeres (Razzaq et al., 2001). Slmap may
532 either bind or recruit Dlg5 to the membrane, the latter was interestingly also found to

533 bind to Mst1 (Hippo homolog) in mammalian cell culture (Kwan et al., 2016), which may
534 boost the interaction of STRIPAK with Hippo, resulting in its effective de-
535 phosphorylation. A detailed molecular model of Hippo signalling (Figure 9) remains
536 speculative to date until the precise subcellular localisation of the key components, Hippo,
537 Slimp and Dlg5 have been resolved in developing muscle.

538

539 **A speculative model how myofibrillogenesis may coordinate with transcription**

540 We have shown that mechanical tension in flight muscles increases during the early
541 phases of myofiber development and identified it as a key regulator of myofibril
542 assembly in flight muscle (Weitkunat et al., 2014). Concomitantly, transcription of
543 sarcomeric components needs to be up-regulated to allow myofibril assembly and
544 myofibril maturation. An attractive although speculative model places the Hippo pathway
545 central to coordinate the assembly status of the myofibrils with the transcriptional status
546 of the muscle fiber nuclei (Figure 9). In analogy to the epithelial cell cortex, we
547 hypothesize that mechanical stretch produced by the actin cytoskeleton potentially via
548 membranes, STRIPAK and Dlg5 may inhibit Hippo and thus promote the nuclear
549 localisation of Yorkie, which in turn will boost transcription of mRNAs coding for
550 sarcomeric components. This would be an analogous mechanism to the inhibition of
551 Hippo by high tension produced by the cortical actomyosin and spectrin networks at the
552 epithelial cortex resulting in epithelial tissue growth (Deng et al., 2015; Fletcher et al.,
553 2015; 2018; Rauskolb et al., 2014). Interestingly, it was shown that filamentous actin (F-
554 actin) levels can directly regulate Hippo pathway activity; more F-actin blocks Hippo
555 signalling, resulting in epithelial tissue over-growth (Fernández et al., 2011; Sansores-

556 Garcia et al., 2011; Yin et al., 2013). A similar feedback loop may enable the induction of
557 more actin and myosin once the myofibrils have started to assemble and produce high
558 levels of mechanical tension (Figure 9). This feedback model implies that only the
559 successful completion of the myofibril assembly step then allows to fully boost
560 sarcomeric mRNA transcription and translation to enable myofibril maturation and
561 muscle fiber growth. This is consistent with the temporal separation of myofibril
562 assembly and maturation in flight muscles (González-Morales et al., 2019; Shwartz et al.,
563 2016; Spletter et al., 2018) Mechanical control of the Hippo pathway and YAP/TAZ
564 localisation by the actomyosin cytoskeleton is also prominent in mammalian cells
565 (Dupont et al., 2011; Wada et al., 2011). A similar mechanical feedback model as
566 proposed here may therefore also be a relevant mechanism to coordinate post-mitotic
567 cardiomyocyte and skeletal muscle growth or regeneration in mammals.

568

569

570

571 **Methods**

572 *Fly strains and genetics*

573 Fly strains were maintained using standard conditions. Unless otherwise stated, all
574 experiments were performed at 27°C to improve RNAi efficiency. When applying
575 temperature sensitive *Tub-GAL80ts*, fly crosses were kept at 18°C to suppress GAL4
576 activity and the white pre-pupae (0-30 min APF) were shifted to 31°C to allow GAL4
577 activity only at pupal stages. The pupae were then raised at 31°C until the desired age.
578 Considering that pupae develop faster at 31°C compared to 27°C, timing was corrected
579 by growing pupae at 31°C for 30 h age matching 32 h APF at 27°C, for 44 h matching
580 48 h APF and for 84 h matching 90 h APF at 27°C. The *Act88F-GAL4 UAS-Hippo* pupae
581 were raised for 66 h at 18°C age matching 32 h APF at 27°C, and for 96 h at 18°C age
582 matching 48 h APF at 27°C. RNAi stocks used were from the Vienna (Dietzl et al., 2007)
583 or Harvard collections (Ni et al., 2011) and obtained from VDRC or Bloomington stock
584 centers. All used fly strains are listed in Supplementary Table 4.

585

586 *Flight*

587 Flight tests were performed as previously described (Schnorrer et al., 2010). One to three
588 day old male flies were dropped into a 1 m long plexiglass cylinder with 8 cm diameter
589 and 5 marked sections. Wild-type flies land in the upper 2 sections, whereas flies with
590 defective flight muscles fall to the bottom of the tube immediately. For each genotype
591 flight assays were performed two or three times with minimum 7 males each (for *yorkie-*
592 *IR* females were used) (Supplementary Table 1).

593

594 *Pupal dissection and flight muscle stainings*

595 For 24 h, 32 h and 48 h APF pupal dissections, the pupa was stabilized on a slide by
596 sticking to double-sticky tape. The pupal case was removed with fine forceps. Using
597 insect pins 2 or 3 holes were made in the abdomen to allow penetration of the fixative
598 and pupae were fixed in 4% PFA (Paraformaldehyde) in PBST (PBS with 0.3% Triton-
599 X) in black embryo glass dishes for 15 min at room temperature (RT). After one wash
600 with PBST the pupae were immobilised using insect pins in a silicone dish filled with
601 PBST and dissected similarly as described previously (Weitkunat and Schnorrer, 2014).
602 Using fine scissors the ventral part of each pupa was removed, then the thorax was cut
603 sagittally and the thorax halves were freed from the abdomen, leaving half thoraces with
604 the flight muscles on them. These half thoraces were transferred to black embryo dishes
605 and blocked for 30 min at room temperature (1/30 normal goat serum in PBST). F-actin
606 was visualised with rhodamine-phalloidin (Molecular Probes, 1/500 in PBST) either
607 alone or in combination with GFP-booster conjugated with Atto488 (ChromoTek, 1/200
608 in PBST) to visualise GFP fusion proteins. Half thoraces were incubated either 1 h at
609 room temperature or overnight at 4°C. After 3 washes with PBST, half thoraces were
610 mounted using Vectashield including DAPI (Biozol).

611 For 90 h APF pupal dissections, the head, wings, legs and abdomen were cut off
612 the thorax with fine scissors, and the thoraxes were fixed for 20 min in 4% PFA in PBST
613 at RT. After washing once with PBST, the thoraxes were placed on a slide with double-
614 sticky tape and cut sagittally (dorsal to ventral) with a microtome blade (Pfm Medical
615 Feather C35). These half thoraces were stained similarly to the early pupa half thoraces
616 and mounted in Vectashield with DAPI using 2 spacer coverslips on each side.

617

618 *Image acquisition and processing*

619 Image acquisition was performed with Zeiss LSM780 or LSM880-I-NLO confocal
620 microscopes using Plan Neofluar 10x/0.30 NA air, Plan-Apo 40x /1.4 NA oil and Plan-
621 Apo 63x/1.4 NA oil objectives. For all samples z-stacks were acquired. Image processing
622 was done using Fiji (Schindelin et al., 2012). Digital cross-sections were created from z-
623 stacks that covered the entire width of the flight muscle by drawing a straight line in the
624 central part of the fiber and re-slicing. Fiber length and fiber cross-sectional area were
625 measured with freehand drawing tools in Fiji based on phalloidin staining. To determine
626 the average muscle fiber length per hemithorax, the length of all flight muscles for which
627 both fiber ends were visible were measured and averaged.

628

629 *Myofibril length quantification and intensity profile plots*

630 Myofibrils stained with phalloidin from a 40 μm x 20 μm x 2.5 μm confocal microscope
631 stack were traced manually using Simple Neurite Tracer plug-in in Fiji (Longair et al.,
632 2011). In each pupa, 10 myofibrils were traced and their average length was calculated.
633 To visualise sarcomere periodicity, intensity profiles were plotted along a line based on
634 actin labelling (phalloidin) using Fiji.

635

636 *Nuclei count*

637 To count nuclei numbers of flight muscle fibers, half thoraces were stained with
638 phalloidin (actin) and DAPI (nuclei) and imaged first using 10x objective to quantify the
639 entire length of the fiber and then with 63x oil objective to visualize details. The acquired

640 63x z-stacks contain the entire muscle depth and about half of the muscle fiber length.
641 Using Fiji's multi-point tool all the nuclei in each z-stack were counted manually, using
642 actin labelling as a landmark to visualize the borders of the fiber. Nuclei number for the
643 entire fiber was calculated using the length of the entire fiber from the 10x image.

644

645 *Cryo cross-sections*

646 Cryo cross-sections were performed as described previously (Spletter et al., 2018).
647 Briefly, the pupal case was removed by fine forceps. Using insect pins 2 or 3 holes were
648 made in the abdomen to allow penetration of the 4% PFA in PBST (PBS with 0.5%
649 Triton-X) overnight at 4°C. Fixed pupae were sunk in 30% sucrose solution in PBST on a
650 nutator at 4°C. Pupae were embedded in O.C.T. compound in plastic moulds (#4566,
651 Sakura Finetek) and frozen on dry ice. Blocks were sectioned at 20 µm thickness on a
652 microtome cryostat. Sections were adhered on glass slides coated with 1% gelatin, 0.44
653 mM chromium potassium sulfate dodecahydrate to improve tissue adherence. Sections on
654 the slide were fixed for 1 minute in 4% PFA with PBS at room temperature, washed once
655 for 5 minutes in PBS, incubated with rhodamine-phalloidin (1/500 in PBST) for 2 h at RT
656 in a wet chamber, washed three times with PBST and mounted in Fluoroshield with
657 DAPI.

658

659 *Quantifying GFP protein levels*

660 GFP-tagged genomic fosmid fly lines (fTRG500 for Mhc-GFP and fTRG10028 for
661 Act88F-GFP) (Sarov et al., 2016) were used for comparison of protein levels in *Mef2*-
662 GAL4 driven knockdown of *yorkie* or gain of function *yorkie-CA* to *Mef2*-GAL4 control.

663 Pupae of the different genotypes were dissected, stained and imaged on the same day in
664 parallel under identical settings (master mixes for staining reagents, identical laser and
665 scanner settings for imaging). Per hemi-thorax one or two different areas were imaged
666 using 63x oil objective, zoom factor 2. In Fiji, five z planes at comparable positions in the
667 muscles were selected for an average intensity projection of the volume into a 2D plane.
668 In the 2D plane, two or three regions of $50 \mu\text{m}^2$ occupied by myofibrils (based on actin
669 labelling) were selected. Mean intensities of each of these regions were averaged to
670 calculate one value per hemi-thorax used for the quantification graphs. For each
671 experimental day, the mean intensity of all wild type samples was set to 1 to calculate the
672 relative intensity of the other genotypes. Data from a minimum of two independent
673 experiments were plotted.

674

675 *RNA-isolation from developing flight muscle*

676 For each replicate, flight muscles from seven *Mef2-GAL4, UAS-GFP-GMA* pupae at 24 h
677 or 32 h APF were dissected in ice-cold PBS treated with DEPC using a fluorescent
678 binocular. Flight muscles were collected in an Eppendorf tube and centrifuged at 2000 g
679 for 5 min. The flight muscle pellet was re-suspended in TRIzol™, shock-frozen in liquid
680 nitrogen and kept at -80°C .

681 RNA was isolated directly from the TRIzol muscle samples using a 96 well plate
682 extraction kit (Direct-zol™-96 RNA, Zymo Research, #R2054): after thawing to room
683 temperature in 1,5 ml Eppendorf tubes, the tissue samples were homogenized using a
684 small pestle, followed by nucleic acid precipitation with 100% ethanol. This suspension
685 was then transferred to the 96-well plate containing the purification columns. DNA

686 digestion was performed ‘in column’ according to the kit instructions. Total RNA was
687 eluted with 25 µl of RNase-free water and was quantified using the Quantifluor RNA
688 System (Promega, #E3310).

689

690 *BRB-sequencing library preparation*

691 RNA sequencing libraries were prepared using 20 ng of total RNA following the BRB-
692 sequencing protocol (Alpern et al., 2019). Briefly, each RNA sample was reverse
693 transcribed in a 96-well plate using SuperScript™ II Reverse Transcriptase (Lifetech
694 18064014) with individual barcoded oligo-dT primers (Microsynth, Switzerland. For
695 primer sequences see (Alpern et al., 2019)). Next, the samples were split into 3 pools,
696 purified using the DNA Clean and Concentrator kit (Zymo Research #D4014), and
697 treated with exonuclease I (New England BioLabs, NEB #M0293S). Double-stranded
698 cDNA was generated by the second strand synthesis via the nick translation method. For
699 that, a mix containing 2 µl of RNase H (NEB, #M0297S), 1 µl of *E. coli* DNA ligase
700 (NEB, #M0205 L), 5 µl of *E. coli* DNA Polymerase (NEB, #M0209 L), 1 µl of dNTP
701 (0.2 mM), 10 µl of 5x Second Strand Buffer (100 mM Tris, pH 6.9, AppliChem,
702 #A3452); 25 mM MgCl₂ (Sigma, #M2670); 450 mM KCl (AppliChem, #A2939); 0.8 mM
703 β-NAD Sigma, N1511); 60 mM (NH₄)₂SO₄ (Fisher Scientific Acros, #AC20587); and
704 11 µl of water was added to 20 µl of ExoI-treated first-strand reaction on ice. The reaction
705 was incubated at 16 °C for 2.5 h. Full-length double-stranded cDNA was purified with
706 30 µl (0.6x) of AMPure XP magnetic beads (Beckman Coulter, #A63881) and eluted in
707 20 µl of water.

708 The Illumina compatible libraries were prepared by tagmentation of 5 ng of full-
709 length double-stranded cDNA with 1 µl of in-house produced Tn5 enzyme (11 µM).
710 After tagmentation the libraries were purified with DNA Clean and Concentrator kit
711 (Zymo Research #D4014), eluted in 20 µl of water and PCR amplified using 25 µl NEB
712 Next High-Fidelity 2x PCR Master Mix (NEB, #M0541 L), 2.5 µl of P5_BRB primer
713 (5 µM, Microsynth), and 2.5 µl of Illumina index adapter (Idx7N5 5 µM, IDT) following
714 program: incubation 72 °C—3 min, denaturation 98 °C—30 s; 15 cycles: 98 °C—10 s,
715 63 °C—30 s, 72 °C—30 s; final elongation at 72 °C—5 min. The fragments ranging 200–
716 1000 bp were size-selected using AMPure beads (Beckman Coulter, #A63881) (first
717 round 0.5x beads, second 0.7x). The libraries were profiled with High Sensitivity NGS
718 Fragment Analysis Kit (Advanced Analytical, #DNF-474) and measured with Qubit
719 dsDNA HS Assay Kit (Invitrogen, #Q32851) prior to pooling and sequencing using the
720 Illumina NextSeq 500 platform using a custom primer and the High Output v2 kit
721 (75 cycles) (Illumina, #FC-404-2005). The library loading concentration was 2.2 pM and
722 sequencing configuration as following: R1 6c / index 8c / R2 78c.

723

724 *Pre-processing of the data—de-multiplexing and alignment*

725 The sample reads de-multiplexing was done using BRB-seqTools
726 (<http://github.com/DeplanckeLab/BRB-seqTools>) as described before (Alpern et al.,
727 2019). The sequencing reads were aligned to the Ensembl gene annotation of the
728 *Drosophila melanogaster* BDGP6.23 genome using STAR (version 020201) (Dobin et al.,
729 2013), and count matrices were generated with HTSeq (version 0.9.1) (Love et al., 2014).

730

731 *Bioinformatics analysis of BRB-Seq data*

732 BRB-seq data quality was assessed in several ways. First, we excluded 5 samples from
733 further analysis due to low numbers of aligned reads (< 500K; removed were 1x 24 h
734 APF wild type, 1x *Dlg5-IR* 24 h, 1x *yorkie-CA* 24h and 2x 32 h APF wild type). Using
735 raw read counts, we performed PCA analysis, calculated heatmaps and Pearson's
736 correlation in R (Version 3.3.1, <https://cran.r-project.org/>). One additional replicate from
737 32 h APF wild type was removed from further analysis as it represented a clear outlier.
738 For the remaining samples, we performed library normalization (RLE) as well as
739 differential expression analysis using DESeq2 (version 1.22.2, (Love et al., 2014)). Genes
740 were considered differentially expressed with a $\log_2FC \geq |1|$ and an $FDR \leq 0.05$.
741 Functional enrichment analysis was performed on the differentially expressed genes
742 using FlyEnrichr (Kuleshov et al., 2019). Data are available at the Gene Expression
743 Omnibus database (Clough and Barrett, 2016), accession number GSE158957.

744

745

746 *Affinity Enrichment Mass Spectrometry*

747 For each replicate, about 100 pupae staged from 24 h - 48 h APF of the genotypes *Mef2-*
748 *GAL4* (control) or *Mef2-GAL4, UAS-Dlg5-GFP* were collected and processed as
749 described previously (Sarov et al., 2016). For each genotype, four replicates (100 pupae
750 each) were snap-frozen in liquid nitrogen and ground to powder while frozen. The
751 powder was processed as described (Hubner et al., 2010). Briefly, the cleared lysate was
752 mixed with magnetic beads pre-coupled to a GFP antibody matrix to perform single step
753 affinity enrichment and mass-spec analysis using an Orbitrap mass spectrometer (Thermo

754 Fisher) and the QUBIC protocol (Hein et al., 2015). Raw data were analysed in
755 MaxQuant version 1.4.3.22 (Cox and Mann, 2008) using the MaxLFQ algorithm for
756 label-free quantification (Cox et al., 2014). The volcano plot was generated with
757 Graphpad.
758
759

760 **Acknowledgements**

761 The authors are indebted to Reinhard Fässler for hosting part of this work in his
762 department, and to Jürg Müller and Anne-Kathrin Classen for hosting A.K.C during parts
763 of this study. We are grateful to the IBDM and LIC (Albert-Ludwigs University of
764 Freiburg) imaging facilities for help with image acquisition and maintenance of the
765 microscopes, we acknowledge the France-BioImaging infrastructure supported by the
766 French National Research Agency (ANR-10-INBS-04-01, Investments for the future).
767 Fly stocks obtained from the Bloomington *Drosophila* Stock Center (NIH
768 P40OD018537) and the Vienna *Drosophila* Resource Center (VDRC) were used in this
769 study. The authors thank Pierre Mangeol and Clara Sidor for helpful discussions and
770 critical comments for this manuscript.

771

772 **Funding**

773 This work was supported by the European Research Council under the European Union's
774 Seventh Framework Programme (FP/2007-2013)/ERC Grant 310939 (F.S.), the Centre
775 National de la Recherche Scientifique (CNRS, A.K.C., B.H.H., F.S., N.M.L.), the
776 excellence initiative Aix-Marseille University A*MIDEX (ANR-11-IDEX-0001-02, F.S.),
777 the French National Research Agency with ANR-ACHN MUSCLE-FORCES (F.S.) and
778 MITO-DYNAMICS (ANR-18-CE45-0016-01, B.H.H., F.S.), the Human Frontiers
779 Science Program (HFSP, RGP0052/2018, F.S.), the Bettencourt Foundation (F.S.), the
780 France-BioImaging national research infrastructure (ANR-10-INBS-04-01), the
781 Humboldt Foundation and EMBO postdoctoral fellowships (A.K.C.) and the Turing
782 Center for Living Systems (CENTURI, A*MIDEX, Investments for the Future).

783 The funders had no role in study design, data collection and analysis, decision to publish,
784 or preparation of the manuscript.

785

786 **Competing interests**

787 The authors declare to have no competing interests relevant to this study.

788

789 **References**

- 790 Alpern, D., Gardeux, V., Russeil, J., Mangeat, B., Meireles-Filho, A.C.A., Breysse, R.,
791 Hacker, D., and Deplancke, B. (2019). BRB-seq: ultra-affordable high-throughput
792 transcriptomics enabled by bulk RNA barcoding and sequencing. *Genome Biology* 20,
793 71–15.
- 794 Avellaneda, J., Rodier, C., Daian, F., Rival, T., Luis, N.M., and Schnorrer, F. (2020).
795 Myofibril and mitochondria morphogenesis are coordinated by a mechanical feedback
796 mechanism in muscle. *bioRxiv* 1–50.
- 797 Bae, S.J., Ni, L., Osinski, A., Tomchick, D.R., Brautigam, C.A., and Luo, X. (2017).
798 SAV1 promotes Hippo kinase activation through antagonizing the PP2A phosphatase
799 STRIPAK. *eLife* 6, e30278.
- 800 Bate, M., Rushton, E., and Currie, D.A. (1991). Cells with persistent twist expression are
801 the embryonic precursors of adult muscles in *Drosophila*. *Development* 113, 79–89.
- 802 Bryantsev, A.L., Baker, P.W., Lovato, T.L., Jaramillo, M.S., and Cripps, R.M. (2012).
803 Differential requirements for Myocyte Enhancer Factor-2 during adult myogenesis in
804 *Drosophila*. *Dev. Biol.* 361, 191–207.
- 805 Carson, J.A., Schwartz, R.J., and Booth, F.W. (1996). SRF and TEF-1 control of chicken
806 skeletal alpha-actin gene during slow-muscle hypertrophy. *Am. J. Physiol., Cell Physiol.*
807 270, C1624–C1633.
- 808 Clough, E., and Barrett, T. (2016). The Gene Expression Omnibus Database. *Methods*
809 *Mol. Biol.* 1418, 93–110.
- 810 Cox, J., and Mann, M. (2008). MaxQuant enables high peptide identification rates,
811 individualized p.p.b.-range mass accuracies and proteome-wide protein quantification.
812 *Nature Biotechnology* 26, 1367–1372.
- 813 Cox, J., Hein, M.Y., Lubner, C.A., Paron, I., Nagaraj, N., and Mann, M. (2014). Accurate
814 proteome-wide label-free quantification by delayed normalization and maximal peptide
815 ratio extraction, termed MaxLFQ. *Mol. Cell Proteomics* 13, 2513–2526.
- 816 Del Re, D.P., Yang, Y., Nakano, N., Cho, J., Zhai, P., Yamamoto, T., Zhang, N., Yabuta,
817 N., Nojima, H., Pan, D., et al. (2013). Yes-associated protein isoform 1 (Yap1) promotes
818 cardiomyocyte survival and growth to protect against myocardial ischemic injury. *J Biol*
819 *Chem* 288, 3977–3988.
- 820 Deng, H., Wang, W., Yu, J., Zheng, Y., Qing, Y., and Pan, D. (2015). Spectrin regulates
821 Hippo signaling by modulating cortical actomyosin activity. *eLife* 4, e06567.
- 822 Dietzl, G., Chen, D., Schnorrer, F., Su, K.-C., Barinova, Y., Fellner, M., Gasser, B.,
823 Kinsey, K., Oppel, S., Scheiblauer, S., et al. (2007). A genome-wide transgenic RNAi
824 library for conditional gene inactivation in *Drosophila*. *Nature* 448, 151–156.

- 825 Dobin, A., Davis, C.A., Schlesinger, F., Drenkow, J., Zaleski, C., Jha, S., Batut, P.,
826 Chaisson, M., and Gingeras, T.R. (2013). STAR: ultrafast universal RNA-seq aligner.
827 *Bioinformatics* 29, 15–21.
- 828 Dong, J., Feldmann, G., Huang, J., Wu, S., Zhang, N., Comerford, S.A., Gayyed, M.F.,
829 Anders, R.A., Maitra, A., and Pan, D. (2007). Elucidation of a universal size-control
830 mechanism in *Drosophila* and mammals. *Cell* 130, 1120–1133.
- 831 Duhart, J.C., and Raftery, L.A. (2020). Mob Family Proteins: Regulatory Partners in
832 Hippo and Hippo-Like Intracellular Signaling Pathways. *Front Cell Dev Biol* 8, 161.
- 833 Dupont, S., Morsut, L., Aragona, M., Enzo, E., Giulitti, S., Cordenonsi, M., Zanconato,
834 F., Le Digabel, J., Forcato, M., Bicciato, S., et al. (2011). Role of YAP/TAZ in
835 mechanotransduction. *Nature* 474, 179–183.
- 836 Dutta, D., Anant, S., Ruiz-Gómez, M., Bate, M., and VijayRaghavan, K. (2004). Founder
837 myoblasts and fibre number during adult myogenesis in *Drosophila*. *Development* 131,
838 3761–3772.
- 839 Ehler, E., and Gautel, M. (2008). The sarcomere and sarcomerogenesis. *Adv. Exp. Med.*
840 *Biol.* 642, 1–14.
- 841 Farrance, I.K., and Ordahl, C.P. (1996). The role of transcription enhancer factor-1 (TEF-
842 1) related proteins in the formation of M-CAT binding complexes in muscle and non-
843 muscle tissues. *Journal of Biological Chemistry* 271, 8266–8274.
- 844 Farrance, I.K., Mar, J.H., and Ordahl, C.P. (1992). M-CAT binding factor is related to the
845 SV40 enhancer binding factor, TEF-1. *Journal of Biological Chemistry* 267, 17234–
846 17240.
- 847 Fernandes, J., Bate, M., and VijayRaghavan, K. (1991). Development of the indirect
848 flight muscles of *Drosophila*. *Development* 113, 67–77.
- 849 Fernández, B.G., Brás-Pereira, C., Rebelo, S.R., and Janody, F. (2011). Actin-Capping
850 Protein and the Hippo pathway regulate F-actin and tissue growth in *Drosophila*.
851 *Development* 138, 2337–2346.
- 852 Fletcher, G.C., Diaz-de-la-Loza, M.-D.-C., Borreguero-Muñoz, N., Holder, M., Aguilar-
853 Aragon, M., and Thompson, B.J. (2018). Mechanical strain regulates the Hippo pathway
854 in *Drosophila*. *Development* 145, dev159467–10.
- 855 Fletcher, G.C., Elbediwy, A., Khanal, I., Ribeiro, P.S., Tapon, N., and Thompson, B.J.
856 (2015). The Spectrin cytoskeleton regulates the Hippo signalling pathway. *The EMBO*
857 *Journal*. 34, 940-954
- 858 Gautel, M. (2008). The sarcomere and the nucleus: functional links to hypertrophy,
859 atrophy and sarcopenia. *Adv. Exp. Med. Biol.* 642, 176–191.

- 860 González-Morales, N., Xiao, Y.S., Schilling, M.A., Marescal, O., Liao, K.A., and Schöck,
861 F. (2019). Myofibril diameter is set by a finely tuned mechanism of protein
862 oligomerization in *Drosophila*. *eLife* 8.
- 863 Goulev, Y., Fauny, J.D., Gonzalez-Marti, B., Flagiello, D., Silber, J., and Zider, A.
864 (2008). SCALLOPED interacts with YORKIE, the nuclear effector of the hippo tumor-
865 suppressor pathway in *Drosophila*. *Current Biology* 18, 435–441.
- 866 Gunage, R.D., Reichert, H., and VijayRaghavan, K. (2014). Identification of a new stem
867 cell population that generates *Drosophila* flight muscles. *eLife* 3, 180–25.
- 868 Hansen, C.G., Ng, Y.L.D., Lam, W.-L.M., Plouffe, S.W., and Guan, K.-L. (2015). The
869 Hippo pathway effectors YAP and TAZ promote cell growth by modulating amino acid
870 signaling to mTORC1. *Cell Res.* 25, 1299–1313.
- 871 Harvey, K., and Tapon, N. (2007). The Salvador-Warts-Hippo pathway - an emerging
872 tumour-suppressor network. *Nat. Rev. Cancer* 7, 182–191.
- 873 Hein, M.Y., Hubner, N.C., Poser, I., Cox, J., Nagaraj, N., Toyoda, Y., Gak, I.A.,
874 Weisswange, I., Mansfeld, J., Buchholz, F., et al. (2015). A Human Interactome in Three
875 Quantitative Dimensions Organized by Stoichiometries and Abundances. *Cell* 163, 712–
876 723.
- 877 Huang, J., Wu, S., Barrera, J., Matthews, K., and Pan, D. (2005). The Hippo signaling
878 pathway coordinately regulates cell proliferation and apoptosis by inactivating Yorkie,
879 the *Drosophila* Homolog of YAP. *Cell* 122, 421–434.
- 880 Hubner, N.C., Bird, A.W., Cox, J., Spletstoesser, B., Bandilla, P., Poser, I., Hyman, A.,
881 and Mann, M. (2010). Quantitative proteomics combined with BAC TransgeneOmics
882 reveals in vivo protein interactions. *The Journal of Cell Biology* 189, 739–754.
- 883 Hwang, J., and Pallas, D.C. (2014). STRIPAK complexes: Structure, biological function,
884 and involvement in human diseases. *International Journal of Biochemistry and Cell*
885 *Biology* 47, 118–148.
- 886 Judson, R.N., Gray, S.R., Walker, C., Carroll, A.M., Itzstein, C., Lionikas, A., Zammit,
887 P.S., De Bari, C., and Wackerhage, H. (2013). Constitutive expression of Yes-associated
888 protein (Yap) in adult skeletal muscle fibres induces muscle atrophy and myopathy. *PLoS*
889 *ONE* 8, e59622.
- 890 Kim, J.H., Jin, P., Duan, R., and Chen, E.H. (2015). Mechanisms of myoblast fusion
891 during muscle development. *Current Opinion in Genetics & Development* 32, 162–170.
- 892 Kuleshov, M.V., Diaz, J.E.L., Flamholz, Z.N., Keenan, A.B., Lachmann, A.,
893 Wojciechowicz, M.L., Cagan, R.L., and Ma'ayan, A. (2019). modEnrichr: a suite of gene
894 set enrichment analysis tools for model organisms. 47, W183–W190.
- 895 Kuleshov, M.V., Jones, M.R., Rouillard, A.D., Fernandez, N.F., Duan, Q., Wang, Z.,

- 896 Koplev, S., Jenkins, S.L., Jagodnik, K.M., Lachmann, A., et al. (2016). Enrichr: a
897 comprehensive gene set enrichment analysis web server 2016 update. *Nucleic Acids Res.*
898 *44*, W90–W97.
- 899 Kwan, J., Sczaniecka, A., Arash, E.H., Nguyen, L., Chen, C.-C., Ratkovic, S., Klezovitch,
900 O., Attisano, L., McNeill, H., Emili, A., et al. (2016). DLG5 connects cell polarity and
901 Hippo signaling protein networks by linking PAR-1 with MST1/2. *Genes &*
902 *Development* *30*, 2696–2709.
- 903 La Marca, J.E., Diepstraten, S.T., Hodge, A.L., Wang, H., Hart, A.H., Richardson, H.E.,
904 and Somers, W.G. (2019). Strip and Cka negatively regulate JNK signalling during
905 *Drosophila* spermatogenesis. *Development* *146*.
- 906 Lemke, S.B., and Schnorrer, F. (2017). Mechanical forces during muscle development.
907 *Mechanisms of Development* *144*, 92–101.
- 908 Lemke, S.B., Weidemann, T., Cost, A.-L., Grashoff, C., and Schnorrer, F. (2019). A
909 small proportion of Talin molecules transmit forces at developing muscle attachments in
910 vivo. *PLoS Biol* *17*, e3000057–29.
- 911 Llewellyn, M., Llewellyn, M.E., Barretto, R.P.J., Barretto, R., Delp, S., Delp, S.L.,
912 Schnitzer, M.J., and Schnitzer, M. (2008). Minimally invasive high-speed imaging of
913 sarcomere contractile dynamics in mice and humans. *Nature* *454*, 784–788.
- 914 Loison, O., Weitkunat, M., Kaya-Copur, A., Nascimento-Alves, C., Matzat, T., Spletter,
915 M.L., Luschnig, S., Brasselet, S., Lenne, P.-F., and Schnorrer, F. (2018). Polarization-
916 resolved microscopy reveals a muscle myosin motor-independent mechanism of
917 molecular actin ordering during sarcomere maturation. *PLoS Biol* *16*, e2004718.
- 918 Longair, M.H., Baker, D.A., and Armstrong, J.D. (2011). Simple Neurite Tracer: open
919 source software for reconstruction, visualization and analysis of neuronal processes.
920 *Bioinformatics* *27*, 2453–2454.
- 921 Love, M.I., Huber, W., and Anders, S. (2014). Moderated estimation of fold change and
922 dispersion for RNA-seq data with DESeq2. *Genome Biology* *15*, 550.
- 923 McGuire, S.E., Le, P.T., Osborn, A.J., Matsumoto, K., and Davis, R.L. (2003).
924 Spatiotemporal rescue of memory dysfunction in *Drosophila*. *Science* *302*, 1765–1768.
- 925 Medioni, C., Ramialison, M., Ephrussi, A., and Besse, F. (2014). Imp Promotes Axonal
926 Remodeling by Regulating profilin mRNA during Brain Development. *Current Biology*
927 *24*, 793–800.
- 928 Neal, S.J., Zhou, Q., and Pignoni, F. (2020). STRIPAK-PP2A regulates Hippo-Yorkie
929 signaling to suppress retinal fate in the *Drosophila* eye disc peripodial epithelium. *Journal*
930 *of Cell Science* *133*, jcs237834.
- 931 Neisch, A.L., Neufeld, T.P., and Hays, T.S. (2017). A STRIPAK complex mediates

- 932 axonal transport of autophagosomes and dense core vesicles through PP2A regulation.
933 *The Journal of Cell Biology* 216, 441–461.
- 934 Ni, J.-Q., Zhou, R., Czech, B., Liu, L.-P., Holderbaum, L., Yang-Zhou, D., Shim, H.-S.,
935 Tao, R., Handler, D., Karpowicz, P., et al. (2011). A genome-scale shRNA resource for
936 transgenic RNAi in *Drosophila*. *Nature Methods* 8, 405–407.
- 937 Oh, H., and Irvine, K.D. (2008). In vivo regulation of Yorkie phosphorylation and
938 localization. *Development* 135, 1081–1088.
- 939 Orfanos, Z., and Sparrow, J.C. (2013). Myosin isoform switching during assembly of the
940 *Drosophila* flight muscle thick filament lattice. *Journal of Cell Science* 126, 139–148.
- 941 Orfanos, Z., Leonard, K., Elliott, C., Katzemich, A., Bullard, B., and Sparrow, J. (2015).
942 Sallimus and the Dynamics of Sarcomere Assembly in *Drosophila* Flight Muscles.
943 *Journal of Molecular Biology* 427, 2151–2158.
- 944 Pan, D. (2010). The hippo signaling pathway in development and cancer. *Developmental*
945 *Cell* 19, 491–505.
- 946 Polesello, C., Huelsmann, S., Brown, N.H., and Tapon, N. (2006). The *Drosophila*
947 RASSF homolog antagonizes the hippo pathway. *Current Biology* 16, 2459–2465.
- 948 Rauskolb, C., Sun, S., Sun, G., Pan, Y., and Irvine, K.D. (2014). Cytoskeletal tension
949 inhibits Hippo signaling through an Ajuba-Warts complex. *Cell* 158, 143–156.
- 950 Razzaq, A., Robinson, I., McMahon, H., Skepper, J., Su, Y., Zelhof, A., Jackson, A., Gay,
951 N., and O’Kane, C. (2001). Amphiphysin is necessary for organization of the excitation–
952 contraction coupling machinery of muscles, but not for synaptic vesicle endocytosis in
953 *Drosophila*. *Genes & Development* 15, 2967.
- 954 Reedy, M.C., and Beall, C. (1993). Ultrastructure of developing flight muscle in
955 *Drosophila*. I. Assembly of myofibrils. *Dev. Biol.* 160, 443–465.
- 956 Regev, G.J., Kim, C.W., Tomiya, A., Lee, Y.P., Ghofrani, H., Garfin, S.R., Lieber, R.L.,
957 and Ward, S.R. (2011). Psoas Muscle Architectural Design, In Vivo Sarcomere Length
958 Range, and Passive Tensile Properties Support Its Role as a Lumbar Spine Stabilizer.
959 *Spine* 36, E1666–E1674.
- 960 Ren, F., Zhang, L., and Jiang, J. (2010). Hippo signaling regulates Yorkie nuclear
961 localization and activity through 14-3-3 dependent and independent mechanisms.
962 *Developmental Biology* 337, 303–312.
- 963 Ribeiro, P.S., Josué, F., Wepf, A., Wehr, M.C., Rinner, O., Kelly, G., Tapon, N., and
964 Gstaiger, M. (2010). Combined functional genomic and proteomic approaches identify a
965 PP2A complex as a negative regulator of Hippo signaling. *Molecular Cell* 39, 521–534.
- 966 Roy, S., and VijayRaghavan, K. (1998). Patterning muscles using organizers: larval

- 967 muscle templates and adult myoblasts actively interact to pattern the dorsal longitudinal
968 flight muscles of *Drosophila*. *Journal of Cell Biology* *141*, 1135-1145.
- 969 Sanger, J.W., Wang, J., Fan, Y., White, J., Mi-Mi, L., Dube, D.K., Sanger, J.M., and
970 Pruyne, D. (2017). Assembly and Maintenance of Myofibrils in Striated Muscle. *Handb*
971 *Exp Pharmacol* *235*, 39–75.
- 972 Sansores-Garcia, L., Bossuyt, W., Wada, K.-I., Yonemura, S., Tao, C., Sasaki, H., and
973 Halder, G. (2011). Modulating F-actin organization induces organ growth by affecting
974 the Hippo pathway. *The EMBO Journal* *30*, 2325–2335.
- 975 Sarov, M., Barz, C., Jambor, H., Hein, M.Y., Schmied, C., Suchold, D., Stender, B.,
976 Janosch, S., K J, V.V., Krishnan, R.T., et al. (2016). A genome-wide resource for the
977 analysis of protein localisation in *Drosophila*. *eLife* *5*, e12068.
- 978 Schiaffino, S. (2018). Muscle fiber type diversity revealed by anti-myosin heavy chain
979 antibodies. *Febs J.* *285*, 3688–3694.
- 980 Schiaffino, S., Dyar, K.A., Ciciliot, S., Blaauw, B., and Sandri, M. (2013). Mechanisms
981 regulating skeletal muscle growth and atrophy. *Febs J.* *280*, 4294–4314.
- 982 Schiaffino, S., Rossi, A.C., Smerdu, V., Leinwand, L.A., and Reggiani, C. (2015).
983 Developmental myosins: expression patterns and functional significance. *Skeletal Muscle*
984 *5*, 22–14.
- 985 Schindelin, J., Arganda-Carreras, I., Frise, E., Kaynig, V., Longair, M., Pietzsch, T.,
986 Preibisch, S., Rueden, C., Saalfeld, S., Schmid, B., et al. (2012). Fiji: an open-source
987 platform for biological-image analysis. *Nature Methods* *9*, 676–682.
- 988 Schnorrer, F., and Dickson, B. (2004). Muscle Building Mechanisms of Myotube
989 Guidance and Attachment Site Selection. *Developmental Cell* *7*, 9–20.
- 990 Schnorrer, F., Schönbauer, C., Langer, C.C.H., Dietzl, G., Novatchkova, M., Schernhuber,
991 K., Fellner, M., Azaryan, A., Radolf, M., Stark, A., et al. (2010). Systematic genetic
992 analysis of muscle morphogenesis and function in *Drosophila*. *Nature* *464*, 287–291.
- 993 Schönbauer, C., Distler, J., Jährling, N., Radolf, M., Dodt, H.-U., Frasch, M., and
994 Schnorrer, F. (2011). Spalt mediates an evolutionarily conserved switch to fibrillar
995 muscle fate in insects. *Nature* *479*, 406–409.
- 996 Shiels, H., and White, E. (2008). The Frank-Starling mechanism in vertebrate cardiac
997 myocytes. *Journal of Experimental Biology* *211*, 2005.
- 998 Shwartz, A., Dhanyasi, N., Schejter, E.D., and Shilo, B.-Z. (2016). The *Drosophila*
999 formin Fhos is a primary mediator of sarcomeric thin-filament array assembly. *eLife* *5*,
1000 D786.
- 1001 Sidor, C., Borreguero-Muñoz, N., Fletcher, G.C., Elbediwy, A., Guillermin, O., and

- 1002 Thompson, B.J. (2019). Mask family proteins ANKHD1 and ANKRD17 regulate YAP
1003 nuclear import and stability. *eLife* 8.
- 1004 Sparrow, J.C., and Schöck, F. (2009). The initial steps of myofibril assembly: integrins
1005 pave the way. *Nature Reviews Molecular Cell Biology* 10, 293–298.
- 1006 Spletter, M.L., Barz, C., Yeroslaviz, A., Schönbauer, C., Ferreira, I.R.S., Sarov, M.,
1007 Gerlach, D., Stark, A., Habermann, B.H., and Schnorrer, F. (2015). The RNA-binding
1008 protein Arrest (Bruno) regulates alternative splicing to enable myofibril maturation in
1009 *Drosophila* flight muscle. *EMBO Rep* 16, 178–191.
- 1010 Spletter, M.L., Barz, C., Yeroslaviz, A., Zhang, X., Lemke, S.B., Bonnard, A., Brunner,
1011 E., Cardone, G., Basler, K., Habermann, B.H., et al. (2018). A transcriptomics resource
1012 reveals a transcriptional transition during ordered sarcomere morphogenesis in flight
1013 muscle. *eLife* 7, 1361.
- 1014 Udan, R.S., Kango-Singh, M., Nolo, R., Tao, C., and Halder, G. (2003). Hippo promotes
1015 proliferation arrest and apoptosis in the Salvador/Warts pathway. *Nature Cell Biology* 5,
1016 914–920.
- 1017 Wackerhage, H., Del Re, D.P., Judson, R.N., Sudol, M., and Sadoshima, J. (2014). The
1018 Hippo signal transduction network in skeletal and cardiac muscle. *Science Signaling* 7,
1019 re4–re4.
- 1020 Wada, K.-I., Itoga, K., Okano, T., Yonemura, S., and Sasaki, H. (2011). Hippo pathway
1021 regulation by cell morphology and stress fibers. *Development* 138, 3907–3914.
- 1022 Watt, K.I., Turner, B.J., Hagg, A., Zhang, X., Davey, J.R., Qian, H., Beyer, C., Winbanks,
1023 C.E., Harvey, K.F., and Gregorevic, P. (2015). The Hippo pathway effector YAP is a
1024 critical regulator of skeletal muscle fibre size. *Nature Communications* 6, 6048–13.
- 1025 Webster, P.J., Liang, L., Berg, C.A., Lasko, P., and Macdonald, P.M. (1997).
1026 Translational repressor bruno plays multiple roles in development and is widely
1027 conserved. *Genes & Development* 11, 2510–2521.
- 1028 Wei, B., Dui, W., Liu, D., Xing, Y., Yuan, Z., and Ji, G. (2013). MST1, a key player, in
1029 enhancing fast skeletal muscle atrophy. *BMC Biol* 11, 12–13.
- 1030 Weitkunat, M., and Schnorrer, F. (2014). A guide to study *Drosophila* muscle biology.
1031 *Methods* 68, 2–14.
- 1032 Weitkunat, M., Brasse, M., Bausch, A.R., and Schnorrer, F. (2017). Mechanical tension
1033 and spontaneous muscle twitching precede the formation of cross-striated muscle in vivo.
1034 *Development* 144, 1261–1272.
- 1035 Weitkunat, M., Kaya-Copur, A., Grill, S.W., and Schnorrer, F. (2014). Tension and
1036 force-resistant attachment are essential for myofibrillogenesis in *Drosophila* flight muscle.
1037 *Curr Biol* 24, 705–716.

- 1038 Willingham, T.B., Kim, Y., Lindberg, E., Bleck, C.K.E., and Glancy, B. (2020). The
1039 unified myofibrillar matrix for force generation in muscle. *Nature Communications* *11*,
1040 3722–10.
- 1041 Wu, S., Huang, J., Dong, J., and Pan, D. (2003). hippo encodes a Ste-20 family protein
1042 kinase that restricts cell proliferation and promotes apoptosis in conjunction with
1043 salvador and warts. *Cell* *114*, 445–456.
- 1044 Wu, S., Liu, Y., Zheng, Y., Dong, J., and Pan, D. (2008). The TEAD/TEF family protein
1045 Scalloped mediates transcriptional output of the Hippo growth-regulatory pathway.
1046 *Developmental Cell* *14*, 388–398.
- 1047 Xu, J., Vanderzalm, P.J., Ludwig, M., Su, T., Tokamov, S.A., and Fehon, R.G. (2018).
1048 Yorkie Functions at the Cell Cortex to Promote Myosin Activation in a Non-
1049 transcriptional Manner. *Developmental Cell* *46*, 271–284.e275.
- 1050 Yin, F., Yu, J., Zheng, Y., Chen, Q., Zhang, N., and Pan, D. (2013). Spatial organization
1051 of Hippo signaling at the plasma membrane mediated by the tumor suppressor
1052 Merlin/NF2. *Cell* *154*, 1342–1355.
- 1053 Zanconato, F., Cordenonsi, M., and Piccolo, S. (2019). YAP and TAZ: a signalling hub
1054 of the tumour microenvironment. *Nat. Rev. Cancer* *1*, 46.
- 1055 Zhang, L., Ren, F., Zhang, Q., Chen, Y., Wang, B., and Jiang, J. (2008). The TEAD/TEF
1056 family of transcription factor Scalloped mediates Hippo signaling in organ size control.
1057 *Developmental Cell* *14*, 377–387.
- 1058 Zheng, Y., Liu, B., Wang, L., Lei, H., Prieto, K.D.P., and Pan, D. (2017). Homeostatic
1059 Control of Hpo/MST Kinase Activity through Autophosphorylation-Dependent
1060 Recruitment of the STRIPAK PP2A Phosphatase Complex. *CellReports* *21*, 3612–3623.
- 1061
- 1062
- 1063

1064 **Figure legends**

1065 **Figure 1. *Dlg5* and *Slmap* are essential for flight muscle morphogenesis**

1066 **A.** Time-course of wild-type dorsal longitudinal indirect flight muscle (DLM)
1067 development. Longitudinal sections (upper panel) of all DLMs and cryo cross-sections
1068 (lower panel) of dorsal longitudinal muscle 4 (DLM4) were stained for actin. Note the
1069 muscle fiber growth in length and width. Scale bars represent 100 μm for longitudinal
1070 and 10 μm for cross-sections. **B.** Longitudinal views of developing flight muscles at 24 h,
1071 32 h, 48 h and 90 h APF of wild type, *Dlg5* or *Slmap* knockdown genotypes (independent
1072 RNAi lines *IR-1* and 2) stained for actin. Note that *Dlg5-IR* and *Slmap-IR* muscles are too
1073 long at 24 h and 32 h APF, and are lost after 32 h APF. The dotted lines highlight the
1074 cuticle. Scale bars represent 50 μm . **C.** Box plot showing flight muscle fiber length at
1075 24 h and 32 h APF of the indicated genotypes. Each dot represents the average muscle
1076 length from one pupa (see Methods). Box extends from 25% to 75%, line marks median,
1077 whiskers extend from max to min, all data points superimposed. Student's t-test, *** p-
1078 value <0.001, *p value <0.05. All following box plots are plotted the same way. $n \geq 8$
1079 pupae for each genotype. **D.** Number of flight muscle fibers in half thoraces at 90 h APF
1080 of the indicated genotypes. Note that *UAS-Dlg5-GFP* but not *UAS-GFP-GMA* rescues the
1081 fiber atrophy phenotype of *Dlg5* knockdown (*Dlg1-IR-1*, in all the following figures *IR*
1082 refers to *IR-1*).

1083

1084 **Figure 1 supplement 1. *Dlg5* and *Slmap* proteins are conserved and required for**
1085 **flight**

1086 **A.** Protein domain organization comparing *Drosophila* Dlg5 to human Dlg5 and
1087 *Drosophila* Dlg1 (isoform M), as well as *Drosophila* Slmap to human Slmap. Note the
1088 conservation of Dlg5 and Slmap between *Drosophila* and human. PDZ: PSD95/Dlg1/ZO-
1089 1 domain; SH3: SRC Homology 3; L27 domain; GuKc: Guanylate kinase domain; FHA:
1090 Forkhead associated domain. **B.** Viability and flight tests of wild type (*Mef2*-GAL4
1091 control) as well as *Dlg5* or *Slmap* knock-down genotypes. Note that knock-down for each
1092 of both genes results in viable but flightless adult flies.

1093

1094 **Figure 2. Dlg5 binds to the STRIPAK complex**

1095 **A.** Volcano plot showing proteins enriched in GFP pull-down from *Mef2*-GAL4, *UAS*-
1096 *Dlg5*-GFP 24 h - 48 h APF pupae. Y-axis shows statistical significance ($-\log_{10}$) and x-
1097 axis the \log_2 fold change (FC) compared to *Mef2*-GAL4 control (see Supplementary
1098 Table 1). STRIPAK complex components are highlighted in red. **B.** Table showing the
1099 \log_2 fold change and p-values of the selected STRIPAK complex components. **C.**
1100 Simplified schematic of the STRIPAK complex (adapted from (Duhart and Raftery,
1101 2020)). Proteins identified in the Dlg5-GFP pull-down are coloured. **D.** Flight muscles at
1102 32 h and 90 h APF of wild type, *Cka* (independent RNAi lines *IR-1* and 2) or *Strip*
1103 knockdown genotypes stained for actin. Note the compaction defect at 32 h APF
1104 followed by muscle atrophy. Scale bars represent 50 μm for 32 h and 100 μm for 90 h
1105 APF. **E.** Box plot showing DLM fiber length at 32h APF of the indicated genotypes.
1106 Each dot is the average from one pupa. Student's t-test, *** p-value <0.001, ** p-value
1107 <0.01.

1108

1109 **Figure 3. The Hippo pathway regulates muscle morphogenesis**

1110 A. Flight muscles at 24 h, 32 h, 48 h and 90 h APF from wild type, *yorkie* knock-down
1111 (independent RNAi lines *IR-1* and 2), *yorkie-CA*, as well as *warts* and *hippo* knockdown
1112 genotypes stained for actin. The dotted lines highlight the cuticle. Note the too long
1113 *yorkie-IR* muscles but too short *yorkie-CA*, *warts-IR* and *hippo-IR* muscles at 24 h and
1114 32 h APF. **B.** Box plot showing muscle fiber length at 24 h and 32 h APF of the
1115 indicated genotypes. Student's t-test, *** p-value<0.001, ** p value<0.01. **C.** Flight
1116 muscles at 32 h and 90 h APF from pupae expressing either wild-type *hippo* or Slmap-
1117 binding deficient *hippo[4A/ 431T]* (under control of the milder tubulin promoter). The
1118 FRT stop cassette is removed by muscle specific *Mef2-GAL4* driven Flp recombinase.
1119 All scale bars represent 50 μ m.

1120

1121 **Figure 3 supplement 1. The Hippo pathway is required for muscle function**

1122 A. Viability and flight tests comparing wild type (*Mef2-GAL4* control) to knockdown or
1123 over-expression of Hippo pathway components. **B.** Cryo cross-sections of dorsal
1124 longitudinal muscle 4 from 24 h and 32 h APF wild type, *Dlg5*, Slmap or *yorkie-IR* and
1125 *yorkie-CA* pupae. Scale bars represent 10 μ m.

1126

1127 **Figure 4. The Hippo pathway is important for post-mitotic muscle development**

1128 **A-D.** Developing flight muscles at 24 h, 32 h, 48 h and 90 h APF from wild type, *Dlg5-*
1129 *IR*, *yorkie-IR* and *yorkie-CA TubGAL80ts Mef2-GAL4* pupae, in which GAL4 activity
1130 was restricted to pupal stages (shift to 31°C at 0 h APF). **A.** Longitudinal sections of all
1131 flight muscles, as well as digital and cryo cross-sections of dorsal longitudinal muscle 4

1132 (DLM4) at 24 h APF. Dotted lines highlight the fiber area. **B.** Box plot displaying DLM4
1133 muscle fiber length, fiber cross-sectional area from digital and cryo sections as well as
1134 the calculated DLM4 fiber volume at 24h APF (calculated by multiplying length with
1135 cross-sectional area from digital cross-sections for each pupa). Student's t-test, *** p-
1136 value<0.001, * p-value<0.05. **C.** Flight muscles at 32 h, 48 h and 90 h APF. Note the too
1137 long muscles in *Dlg5-IR*, *yorkie-IR* at 32 h APF followed by muscle atrophy and the too
1138 short *yorkie-CA* fibers at 32 h that develop disorganised fibers at 90 h APF. **D.** Box plot
1139 illustrating the average muscle fiber length at 32 h APF. Student's t-test, *** p-
1140 value<0.001. **E.** Control and *Act88F-GAL4 UAS-hippo* flight muscles at 32 h and 90 h
1141 APF. Note the induced fiber compaction defect followed by the muscle atrophy. All scale
1142 bars represent 50 μm for longitudinal sections and 10 μm for cross-sections.

1143

1144 **Figure 4 supplement 1. The Hippo pathway is not required for myoblast fusion**

1145 **A.** Quantification of nuclei number of DLM4 at 24 h APF from wild type, *Dlg5-IR*,
1146 *yorkie-IR* and *yorkie-CA TubGAL80ts Mef2-GAL4* (shifted to 31°C at 0 h APF). Fibers
1147 were stained for actin (phalloidin) and nuclei (DAPI). Images illustrating how the nuclei
1148 counting was done using longitudinal sections of DLM4. Since fiber widths vary in
1149 different genotypes, for illustration purposes different numbers of z-planes were
1150 maximum projected to result in comparable volumes. Dotted lines highlight the cell
1151 borders of the fibers. Scale bar represents 20 μm . **B.** Box plot showing total DLM4 nuclei
1152 numbers at 24h. Each dots represents one pupa. Student's t test, n.s. $p > 0.05$.

1153

1154 **Figure 5. The Hippo pathway is essential for post-mitotic muscle fiber growth.**

1155 **A, B.** Longitudinal sections of all DLMs (A) and digital cross-sections of DLM4 (B) at
1156 24 h, 32 h, 48 h and 90 h APF from wild type, *Dlg5-IR*, *yorkie-IR* and *yorkie-CA*
1157 *TubGAL80ts Mef2-GAL4* (shifted to 31°C at 0 h APF) stained for actin. Scale bars
1158 represent 50 µm for longitudinal sections and 10 µm for cross-sections. In B dotted lines
1159 highlight the fiber area. **C.** Box plots showing DLM4 fiber length, digital cross-sectional
1160 area and volume (calculated by multiplying length with cross-sectional area for each
1161 pupa) at 24 h and 48 h APF. Student's t test, *** p-value <0.001, * p-value <0.05.

1162

1163 **Figure 6. The Hippo pathway is essential for myofibrillogenesis**

1164 **A.** Myofibrils visualised by phalloidin from control, *Dlg5-IR* and *yorkie-IR UAS-Diap1*
1165 *TubGAL80ts Mef2-GAL4* muscles at 32 h and 48 h APF (shifted to 31°C at 0 h APF).
1166 The red-boxed areas are magnified. Note the less regular myofibril pattern of *Dlg5-IR*
1167 and *yorkie-IR* muscles at 32 h APF that makes it hard to trace an individual myofibril (see
1168 Figure 6 supplement 1A). Even at 48 h APF, myofibrils from *Dlg5-IR* and *yorkie-IR* are
1169 hard to trace continuously. Scale bars represent 10 µm in the overviews and 2 µm in the
1170 zoomed red boxes. **B.** Box plot of traced myofibril length in a 40 x 20 x 2.5 µm volume
1171 (see Figure 6 supplement 1A). Student's t test, *** p-value <0.001. **C.** Cryo cross-
1172 sections of DLM4 from control, *Dlg5-IR* and *yorkie-IR UAS-Diap1 TubGAL80ts Mef2-*
1173 *GAL4* muscles at 48 h APF (shifted to 31°C at 0 h APF). Yellow dots represent the
1174 myofibrils recognized by the MyofibrilJ plug-in to automatically count the number of
1175 myofibrils per DLM4 fiber (Spletter et al., 2018). Scale bar represents 10 µm. **D.** Box
1176 plot of myofibril number in DLM4 of indicated genotypes at 48 h APF. Student's t test,
1177 *** p-value <0.001. **E.** Flight muscle and myofibril morphologies of wild-type muscles

1178 expressing *yorkie-CA*, *yorkie* or *myr-yorkie* under the control of post-mitotic *Act88F*-
1179 GAL4 at 24 h and 32 h APF. Scale bars represent 50 μm in muscle fiber images and
1180 10 μm in myofibril images.

1181

1182 **Figure 6 supplement 1. Myofibril tracing and nuclei positions in *Dlg5-IR* and *yorkie-***
1183 ***IR* muscles**

1184 **A.** Myofibrils visualised by phalloidin from control, *Dlg5-IR* and *yorkie-IR UAS-Diap1*
1185 *TubGAL80ts Mef2-GAL4* muscles at 32 h and 48 h APF (shifted to 31°C at 0 h APF).
1186 Myofibrils were traced with Simple Neurite Tracer and traces are highlighted in red. Note
1187 that in *Dlg5-IR* and *yorkie-IR* myofibrils traces are short. Scale bars represent 10 μm . **B.**
1188 Flight muscles stained for actin (phalloidin) and nuclei (DAPI) from control, *Dlg5-IR* and
1189 *yorkie-IR UAS-Diap1 TubGAL80ts Mef2-GAL4* muscles at 32 h (shifted to 31°C at 0 h
1190 APF). Note that nuclei fail to distribute between the myofibril bundles but cluster
1191 centrally in *Dlg5-IR* and *yorkie-IR* fibers. Scale bar represents 10 μm . **C.** Box plot of
1192 myofiber cross-sectional areas from cryo cross-sections of DLM4 from control, *Dlg5-IR*
1193 and *yorkie-IR UAS-Diap1 TubGAL80ts Mef2-GAL4* muscles at 48 h APF. Student's t
1194 test, *** p-value <0.001. **D.** Intensity profiles of control myofibrils compared to UAS-
1195 *yorkie-CA*, UAS-wild-type-*yorkie* or UAS-*myr-yorkie* expressed with the post-mitotic
1196 *Act88F-GAL4* driver at 32 h APF. Note the less pronounced actin periodicity in UAS-*yki*
1197 and UAS-*yki-CA* compared to wild-type control. Scale bars represent 10 μm . **E.** 90 h APF
1198 half thorax from *scalloped-IR Mef2-GAL4*. The dotted lines highlight the cuticle. Scale
1199 bar represents 50 μm .

1200

1201 **Figure 7. Yorkie transcriptionally controls sarcomeric and mitochondrial genes**
1202 **expression**

1203 **A.** Gene ontology (GO)-term enrichments in genes lists that are significantly changed in
1204 the various loss (*Dlg5-IR*, *Slmap-IR*, *yorkie-IR*) and gain of function (*yorkie-CA*, *hippo-*
1205 *IR*) *yorkie* conditions at 24 h and 32 h APF compared to wild-type controls (see
1206 Supplementary Table 3). Note the strong enrichment of sarcomere related GO-terms in
1207 the 24 h APF loss of function and the 32 h APF gain of function condition. 32 h APF gain
1208 of function is also strongly enriched for mitochondrial GO-terms. **B.** Plot displaying the
1209 log₂-fold change of transcript levels for individual genes of the above genotypes
1210 compared to control (up in red, down in blue). Note the strong down-regulation of the
1211 sarcomeric genes in the 24 h APF loss of function conditions, in particular the titin
1212 homologs *bt* and *sls*, as well as *Mhc*, *Prm* and *Act88F*.

1213

1214 **Figure 7 supplement 1. BRB sequencing read counts and PCA analysis**

1215 **A.** Principle component analysis (PCA) of BRB-sequencing replicates. Note the distinct
1216 clustering of 24 h from 32 h APF samples. Most but not all samples of similar genotypes
1217 cluster together. **B.** Transformed read count distributions of the 24 h and 32 h APF
1218 samples.

1219

1220 **Figure 8. Yorkie regulates sarcomere protein expression**

1221 **A, B.** *Mhc*-GFP (**A**) and *Act88F*-GFP (**B**) proteins levels visualised with a GFP
1222 nanobody together with actin comparing wild-type control with *yorkie-IR* and *yorkie-CA*
1223 at 24 h and 32 h APF. Scale bars represent 2 μ m. GFP channel is displayed using the

1224 “fire” look-up table. C. Quantification of relative GFP protein levels compared to wild
1225 type (wild-type mean set to 1 for each individual experiment). Bar plots display average
1226 normalised value and each dot represents one hemithorax. Student’s t test, *** p-value
1227 <0.001, ** p-value <0.01 * p-value <0.05.

1228

1229

1230 **Figure 9. Model of Yorkie’s role how to coordinate myofibrillogenesis with**
1231 **transcription during muscle morphogenesis**

1232

1233 **Supplementary Table 1**

1234 Data table containing data from Figures 1, 2, 3, 4, 5, 6 and 8.

1235

1236 **Supplementary Table 2**

1237 Table listing the expression levels and fold changes as well as normalised p-values of the
1238 BRB-SEQ data compared to the wild-type controls. All or the only the significantly
1239 different genes are listed.

1240

1241 **Supplementary Table 3**

1242 GO enrichment terms of the significantly different gene lists of the various genotypes and
1243 time points.

1244

1245 **Supplementary Table 4**

1246 Table listing all *Drosophila* strains and major reagents used in the study

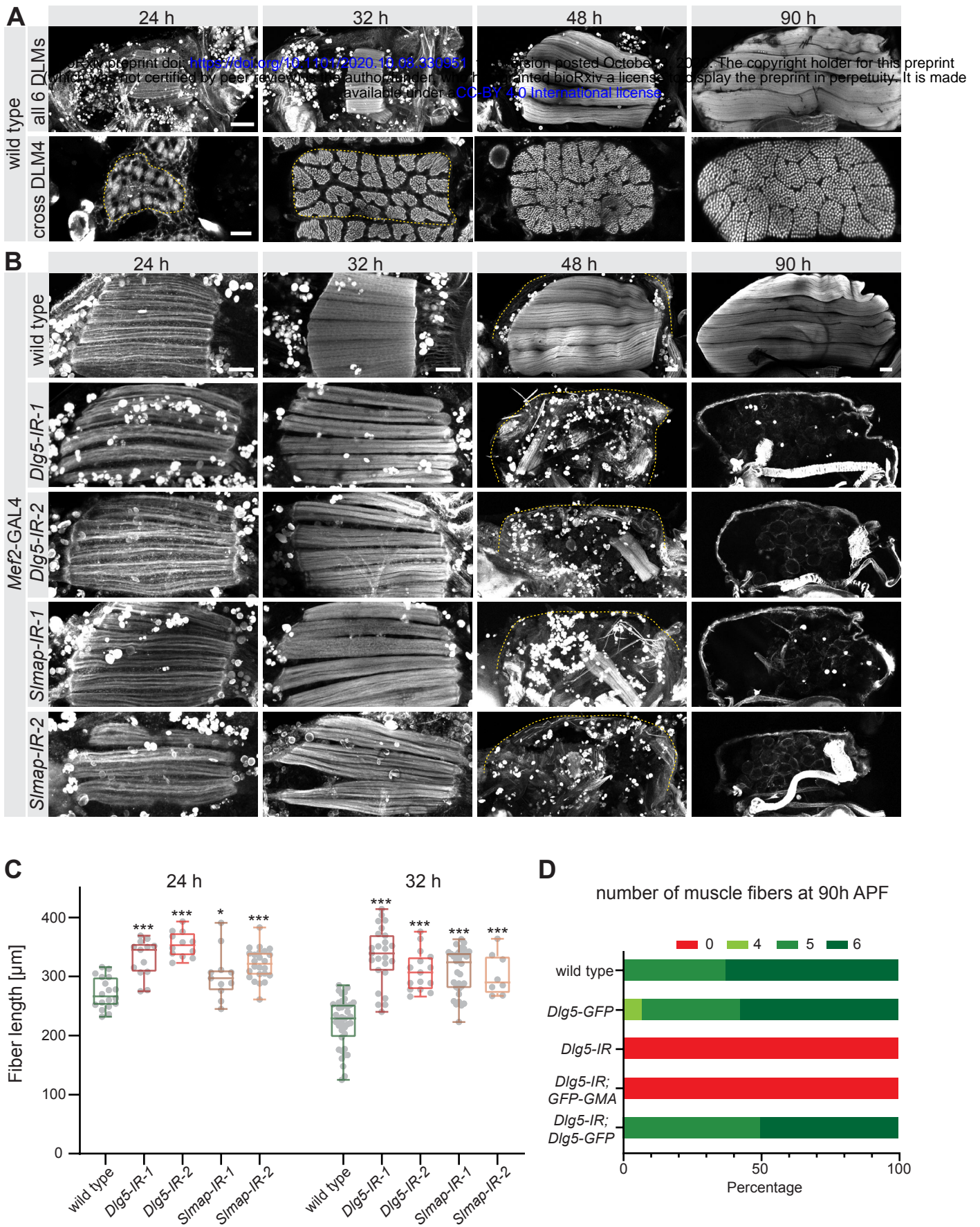


Figure 1

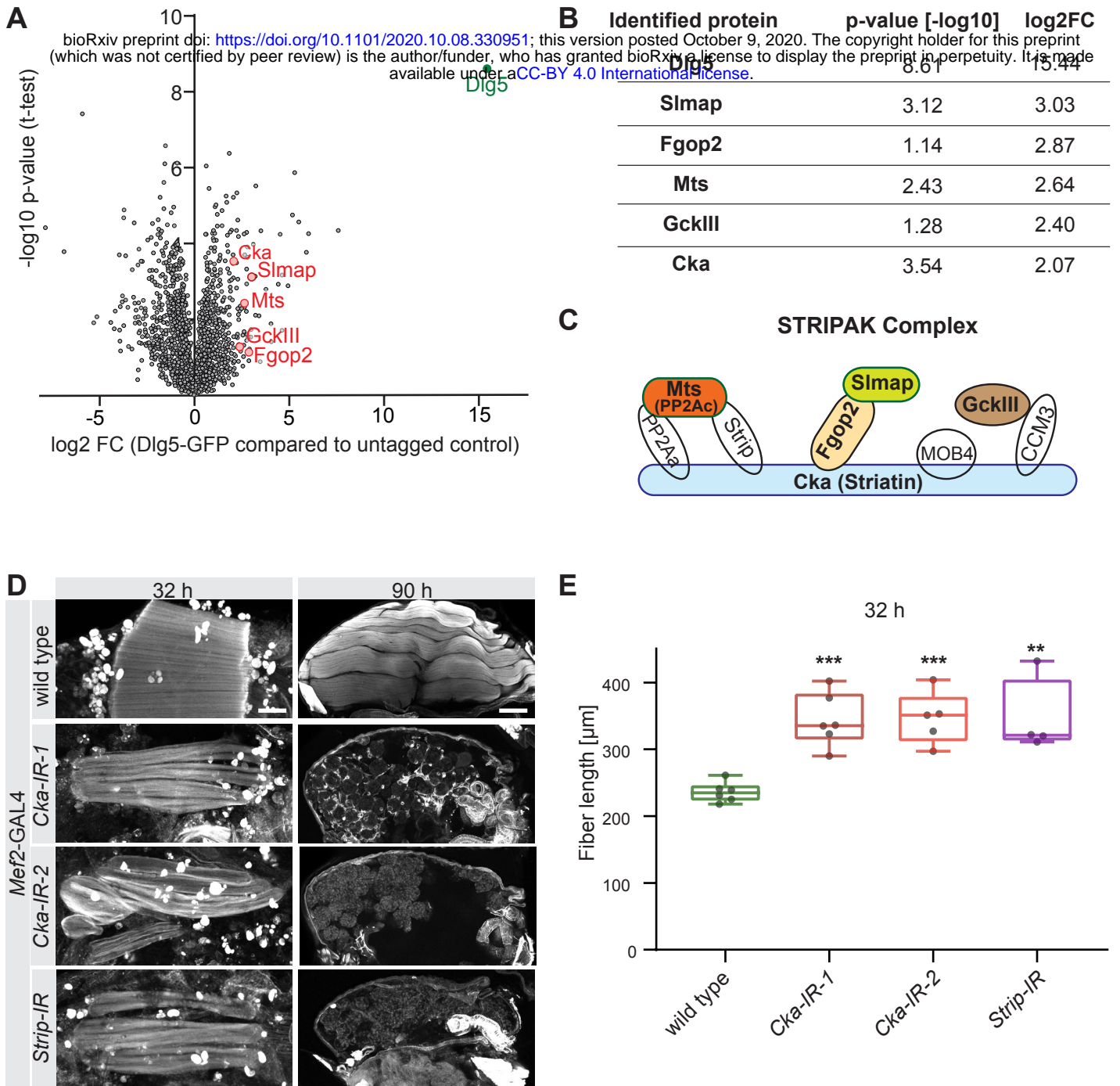


Figure 2

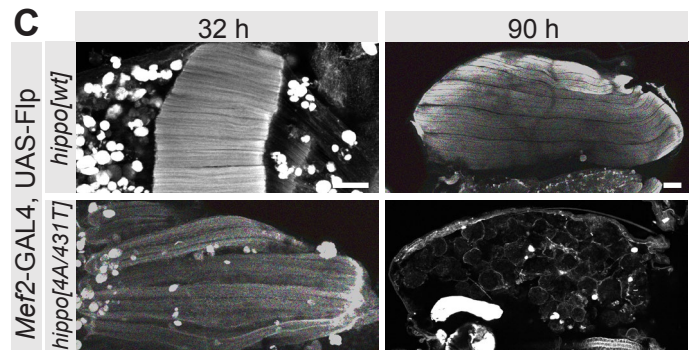
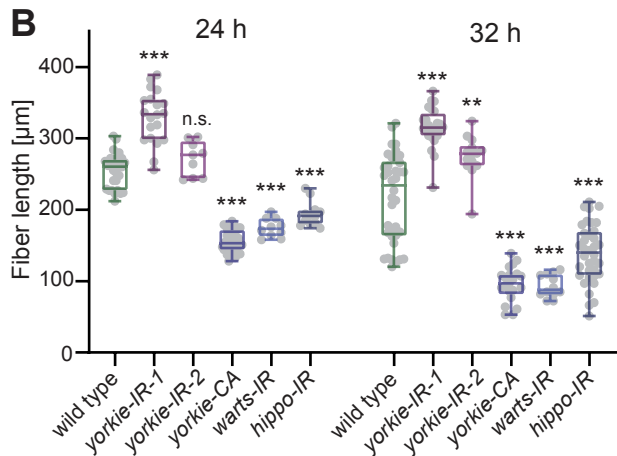
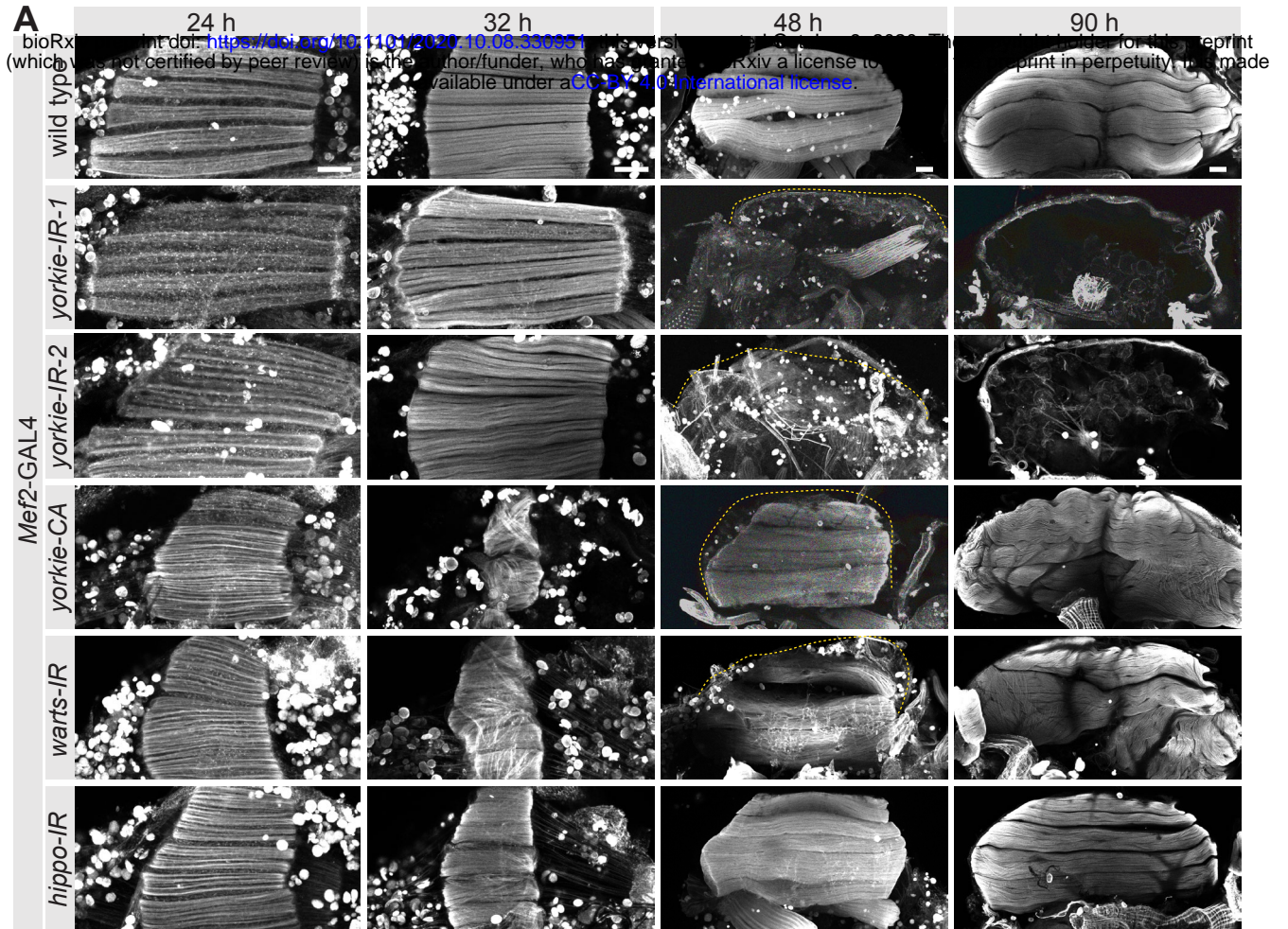
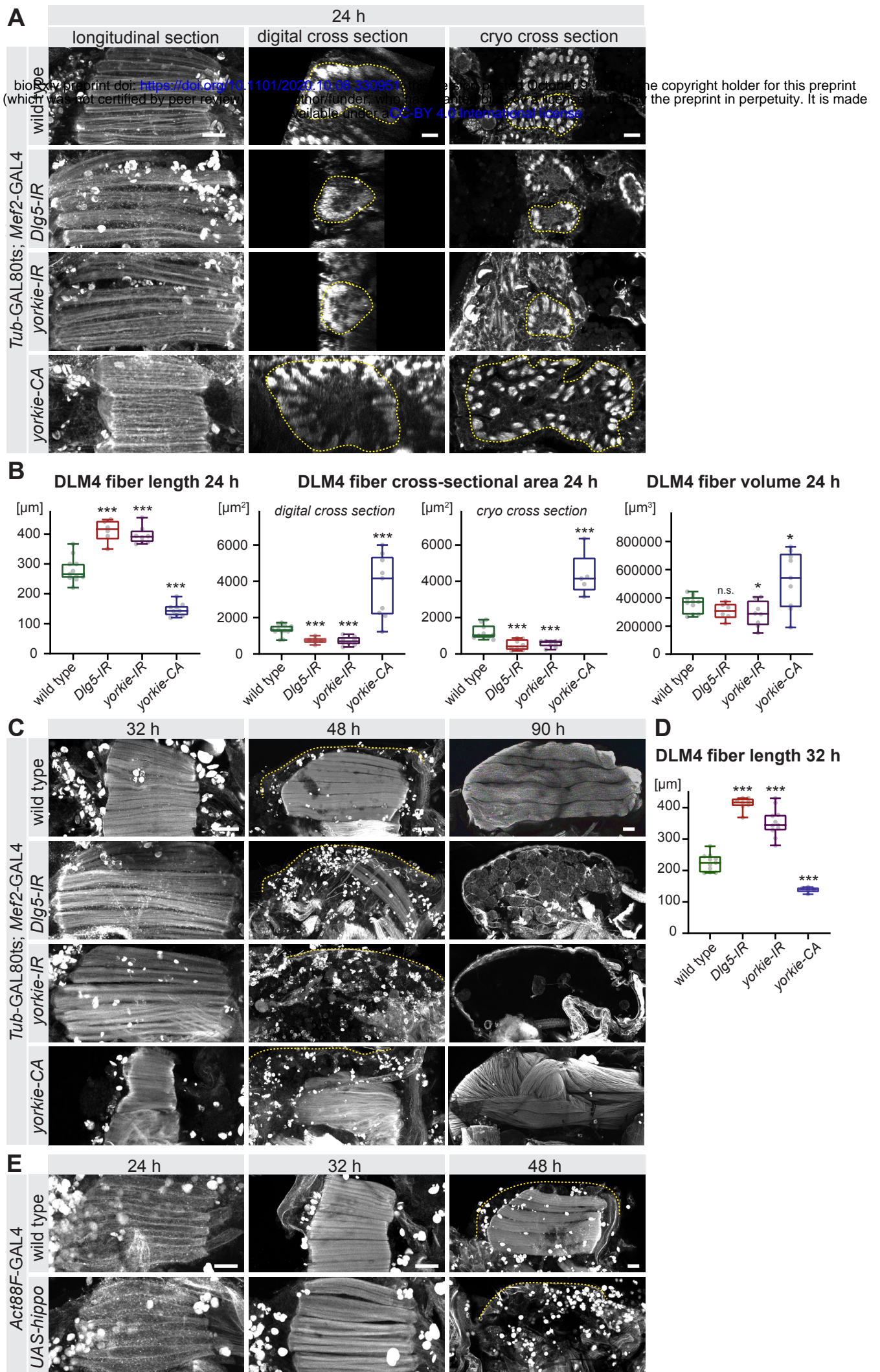


Figure 3



bioRxiv preprint doi: <https://doi.org/10.1101/2021.10.08.330951>; this version posted October 19, 2021. The copyright holder for this preprint (which was not certified by peer review) is the author/funder, who has granted bioRxiv a license to display the preprint in perpetuity. It is made available under aCC-BY 4.0 International license.

The copyright holder for this preprint (which was not certified by peer review) is the author/funder, who has granted bioRxiv a license to display the preprint in perpetuity. It is made available under aCC-BY 4.0 International license.

Figure 4

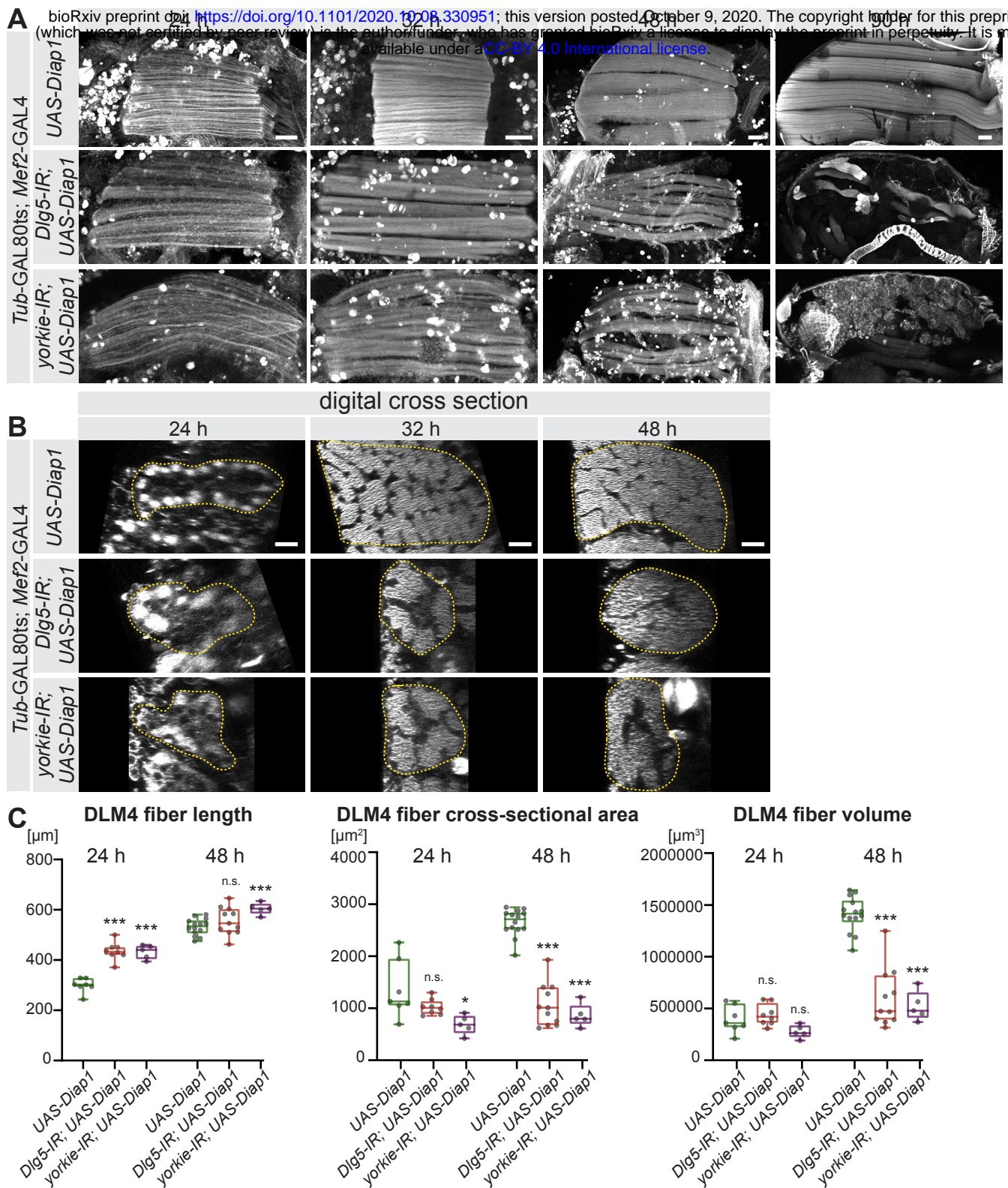


Figure 5

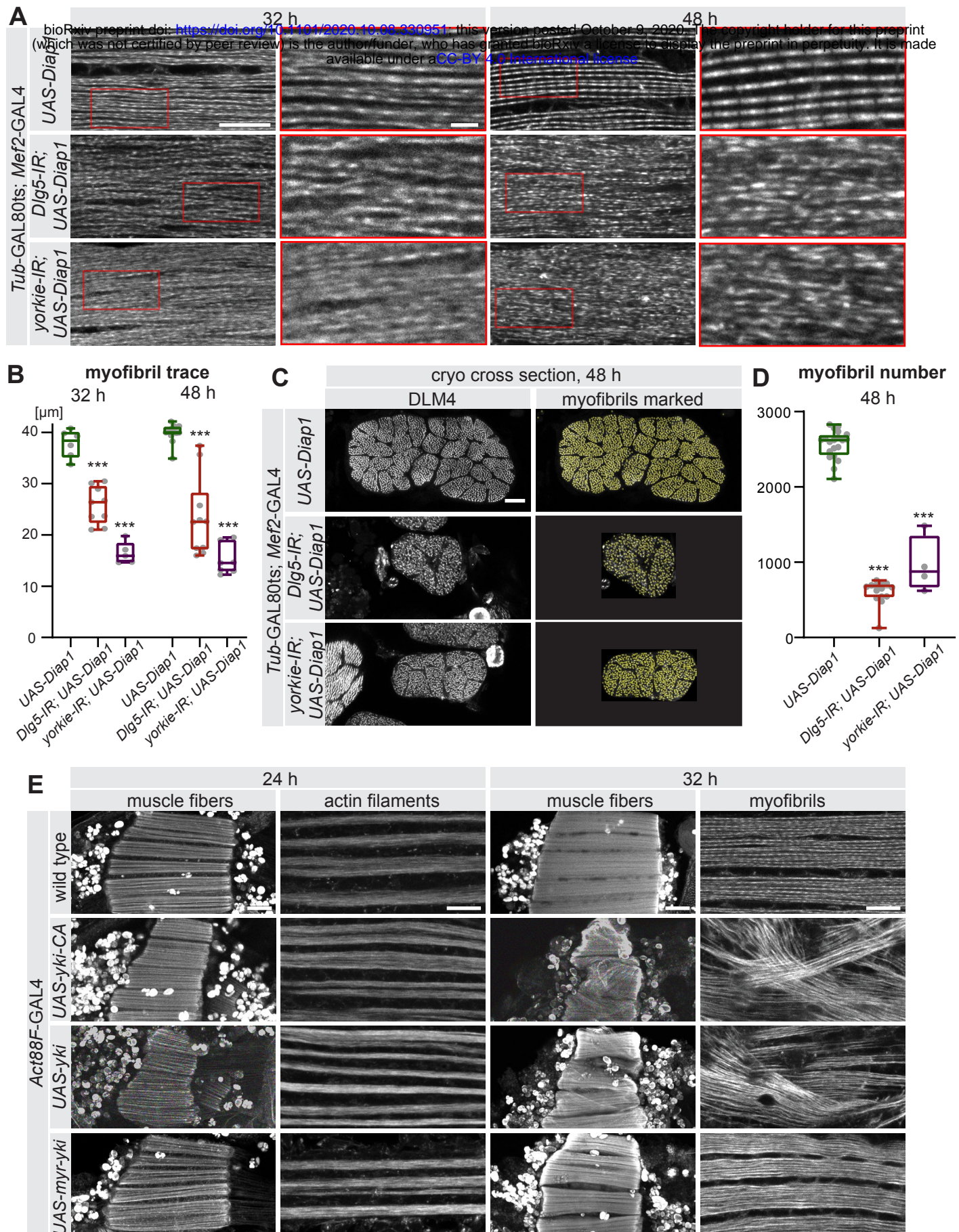


Figure 6

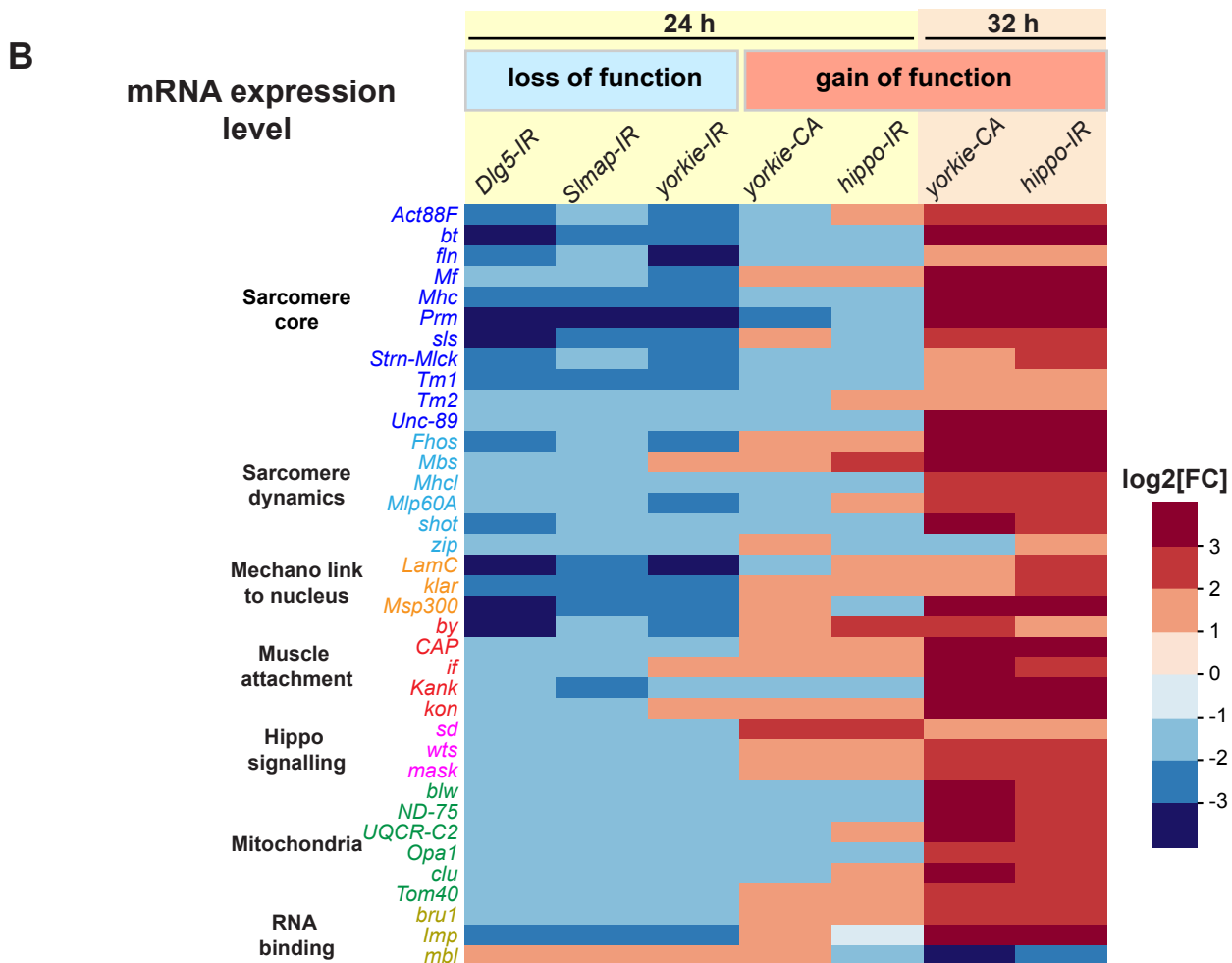
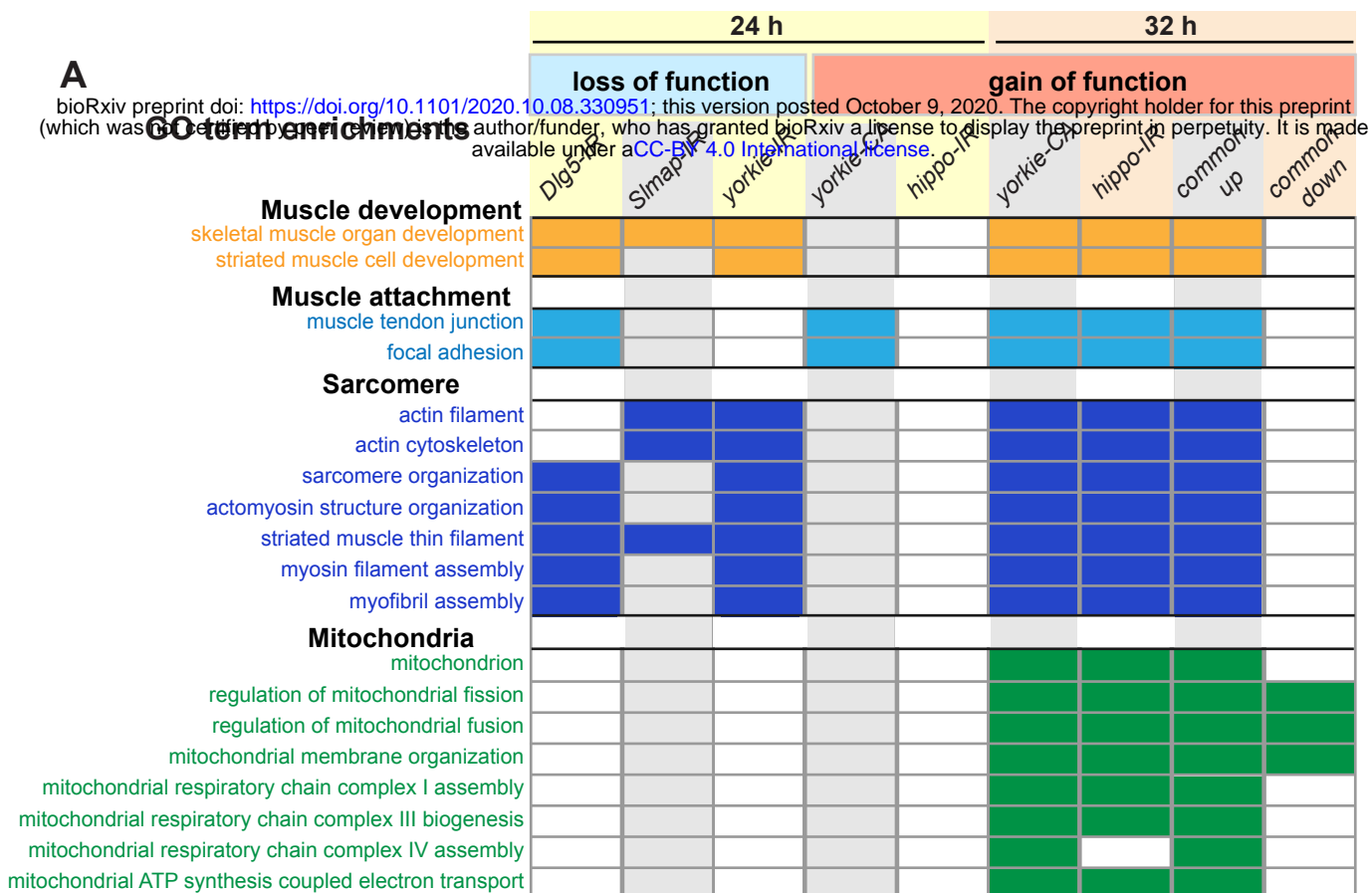


Figure 7

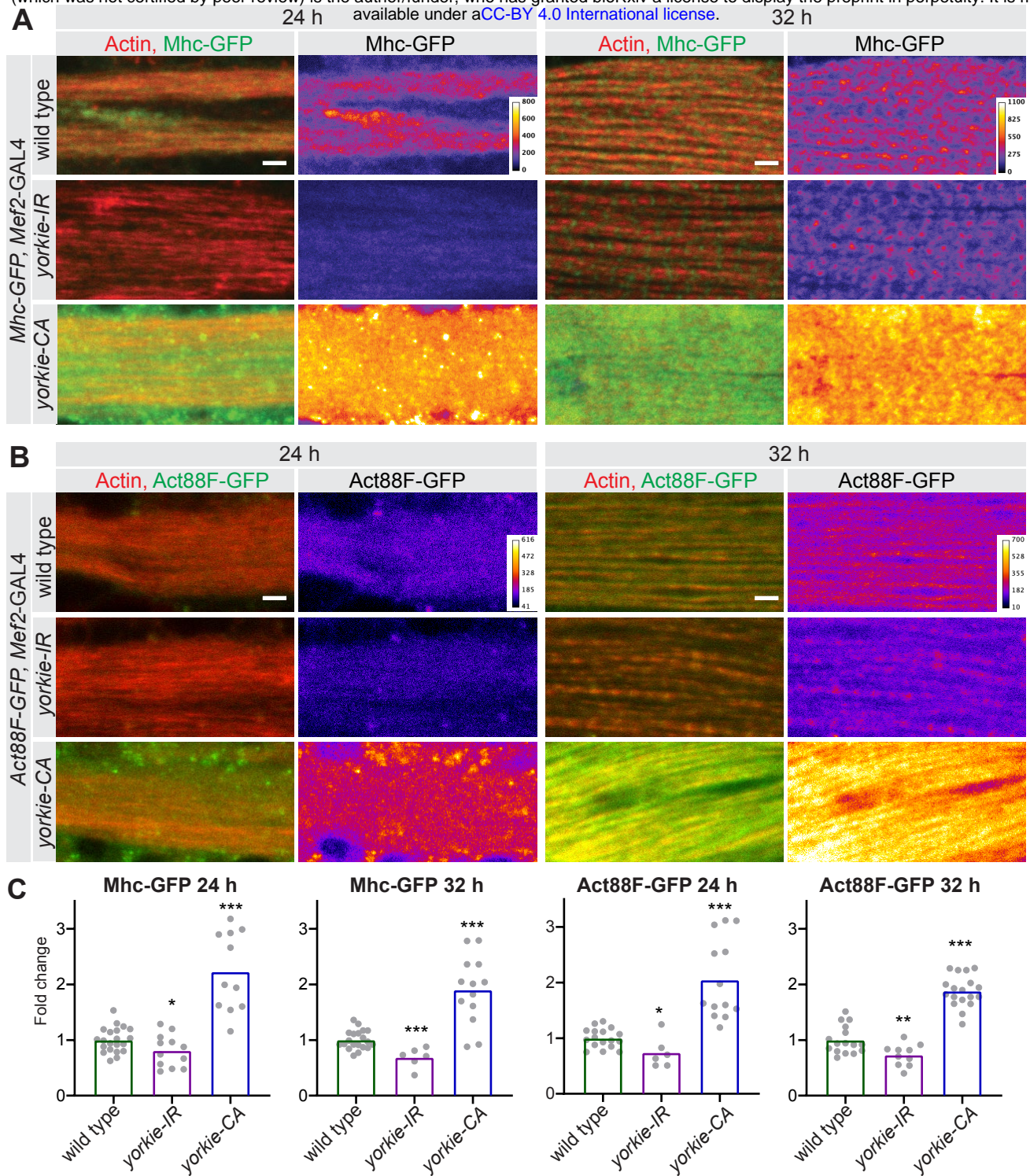


Figure 8

Model: coordination of myofibril morphogenesis with transcription

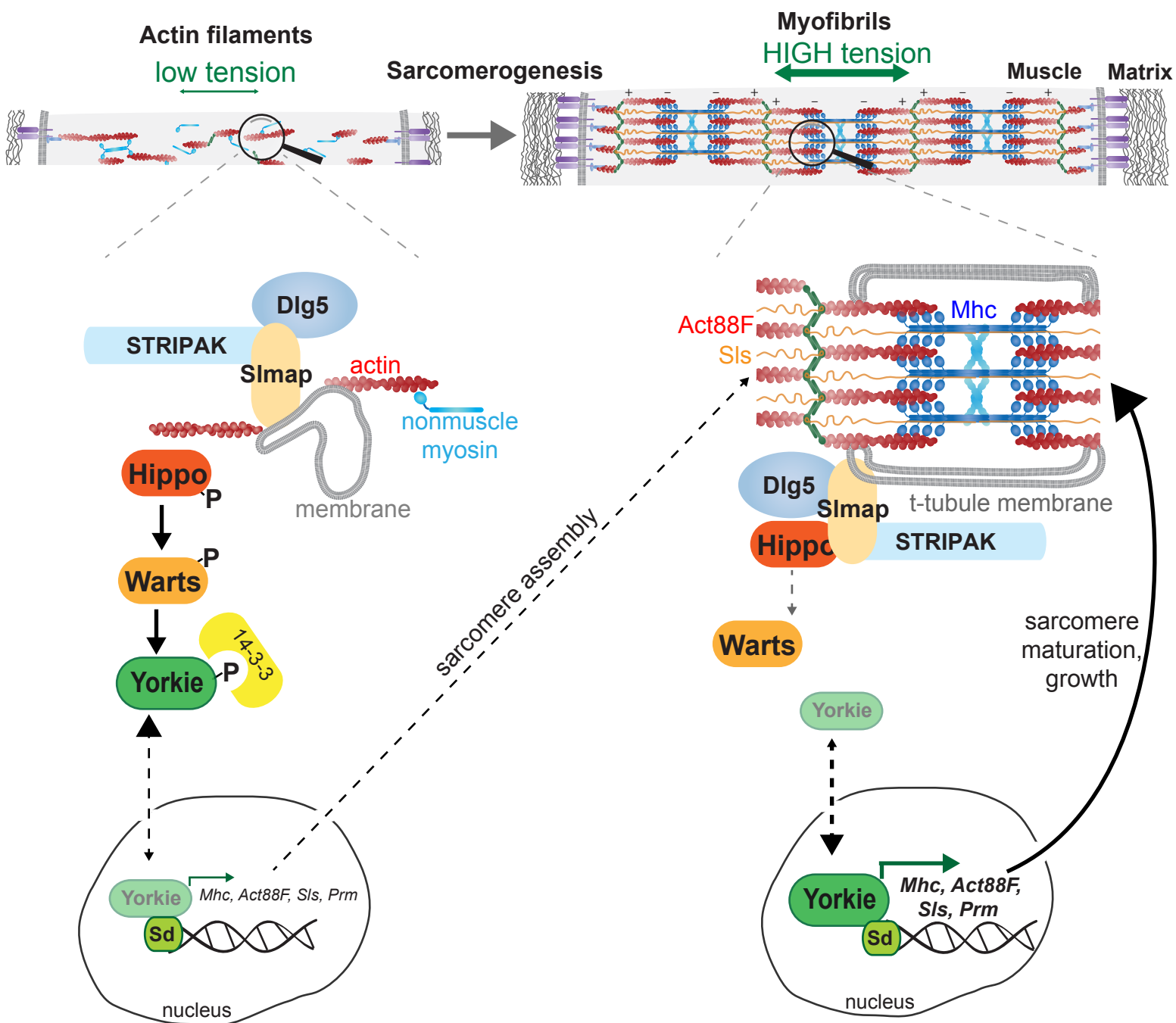
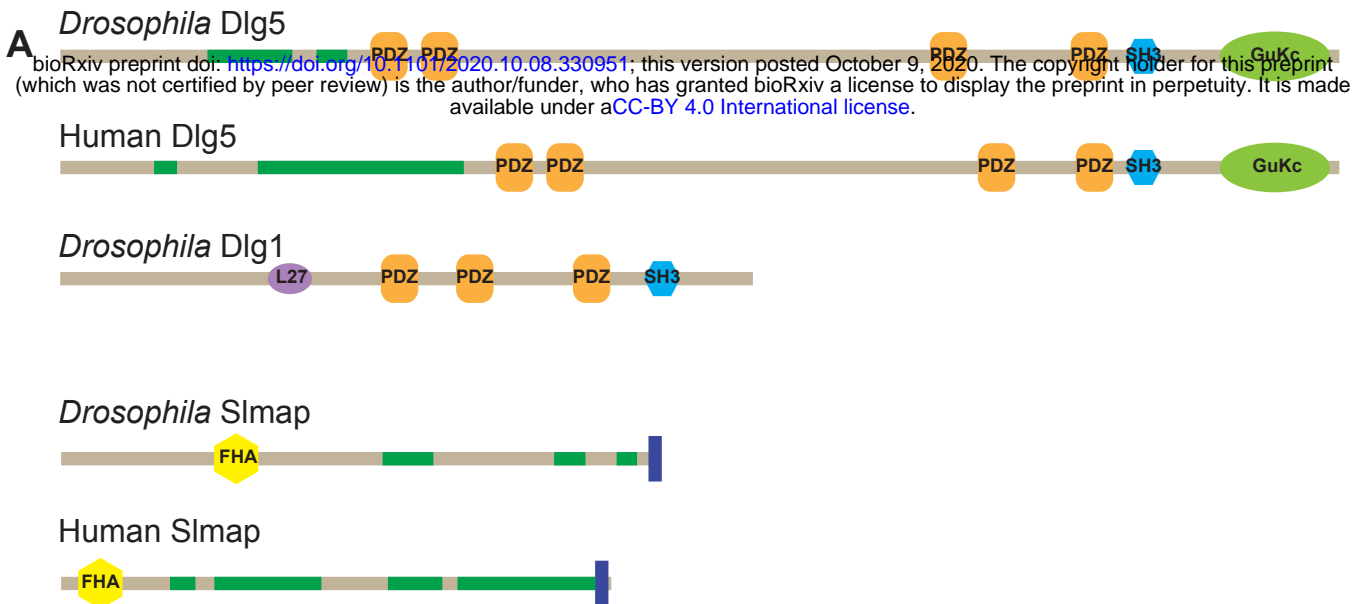


Figure 9



B

Genotype	Phenotype	
	Lethality	Flight
<i>Mef2-GAL4; +</i>	viable	wild type
<i>Mef2-GAL4; Dlg5-IR-1</i> (VDRRC 22496)	viable	flightless
<i>Mef2-GAL4; Dlg5-IR-2</i> (VDRRC 101596)	viable	flightless
<i>Mef2-GAL4; Dlg5-IR-3</i> (BDSC 30925)	viable	flightless
<i>Mef2-GAL4; Slmap-IR-1</i> (VDRRC 8199)	viable	flightless
<i>Mef2-GAL4; Slmap-IR-2</i> (BDSC 32509)	viable	flightless

Figure 1 - Supplement 1

A **Genotype** **Phenotype**
 bioRxiv preprint doi: <https://doi.org/10.1101/2020.10.08.330951>; this version posted October 9, 2020. The copyright holder for this preprint (which was not certified by peer review) is the author/funder, who has granted bioRxiv a license to display the preprint in perpetuity. It is made available under aCC-BY 4.0 International license.

Genotype	viability	flight
<i>Mef2-GAL4; +</i>	viable	wild type
<i>Mef2-GAL4; yorkie-IR-1</i> (VDRC 111001)	male lethal	flightless (females)
<i>Mef2-GAL4; yorkie-IR-2</i> (VDRC 40497)	viable	flightless
<i>Mef2-GAL4; yorkie-CA</i> (S168A)	viable	flightless
<i>Mef2-GAL4; warts-IR-1</i> (VDRC 111002)	pupal lethal	n.a.
<i>Mef2-GAL4; warts-IR-2</i> (BDSC 41899)	pupal lethal	n.a.
<i>Mef2-GAL4; hippo-IR</i> (VDRC 104169)	viable	flightless

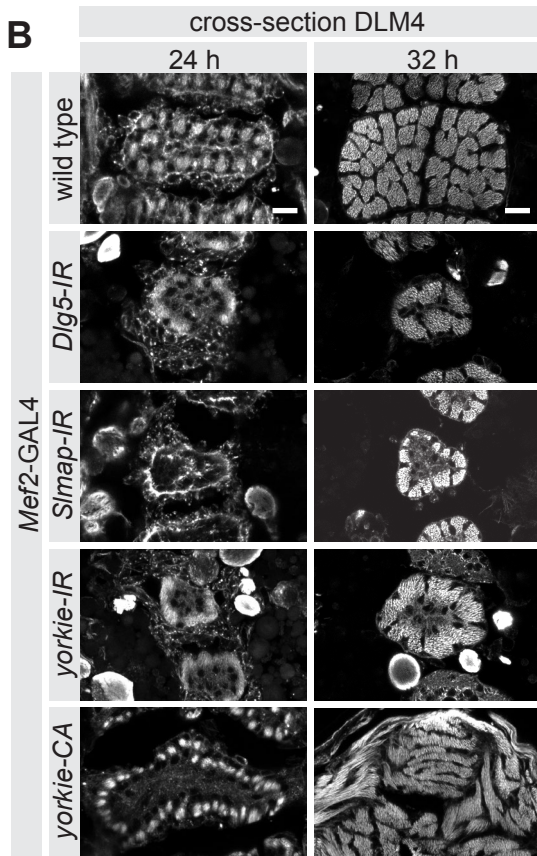


Figure 3 - Supplement 1

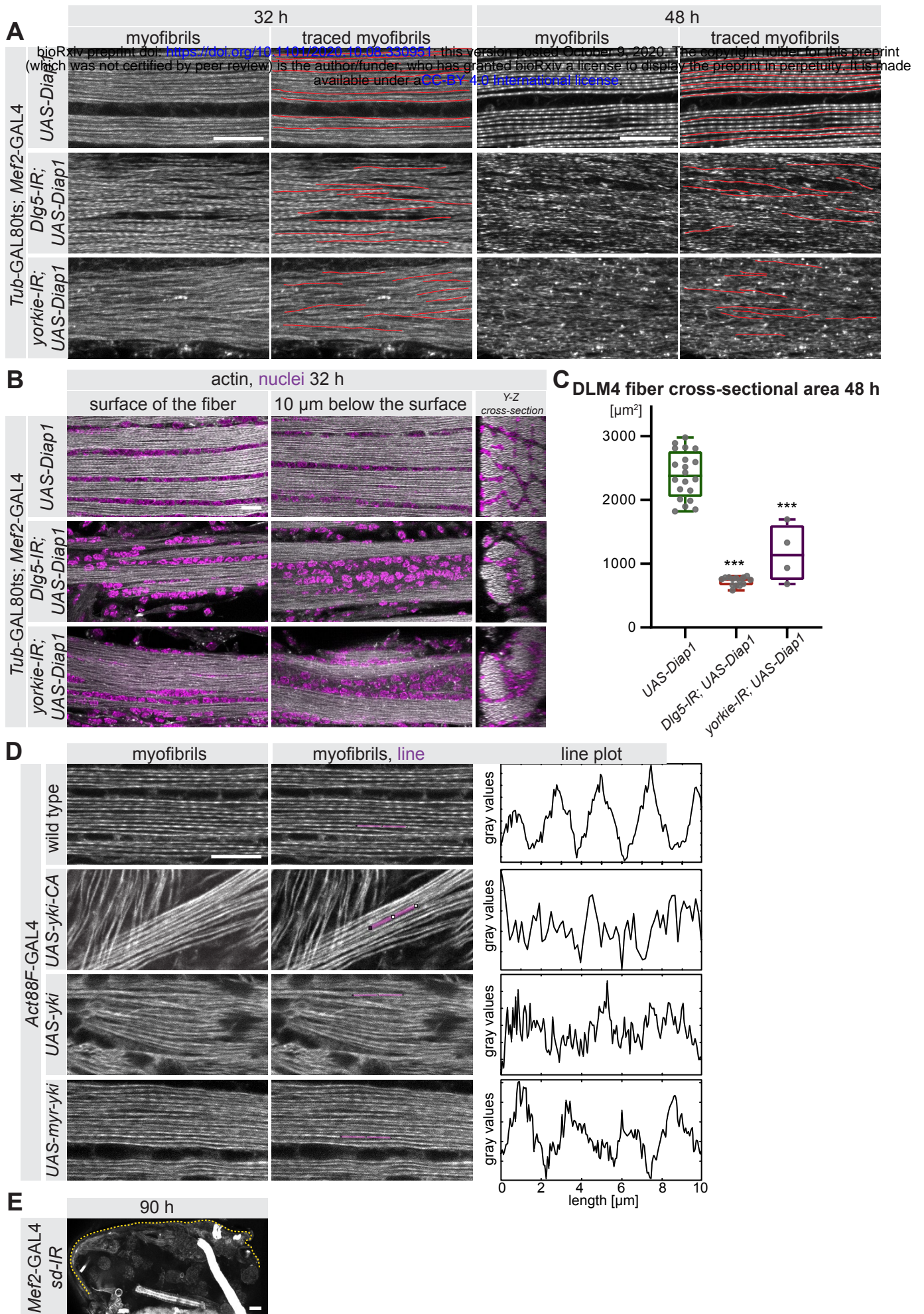


Figure 6 - Supplement 1

A

bioRxiv preprint doi: <https://doi.org/10.1101/2020.10.08.330951>; this version posted October 9, 2020. The copyright holder for this preprint (which was not certified by peer review) is the author/funder, who has granted bioRxiv a license to display the preprint in perpetuity. It is made available under aCC-BY 4.0 International license.

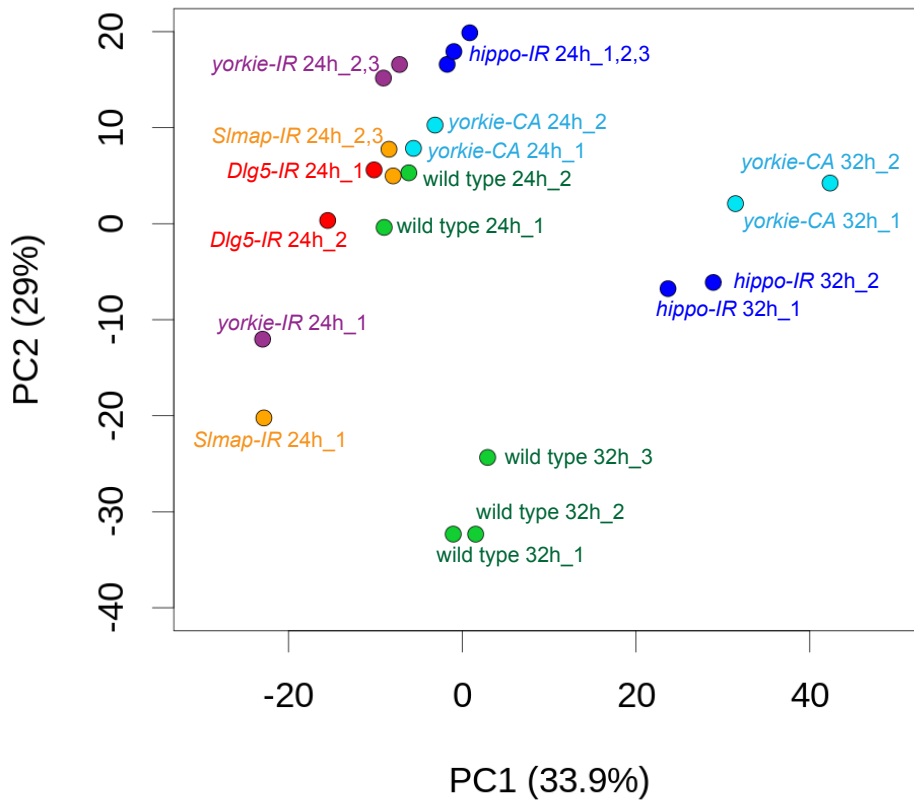
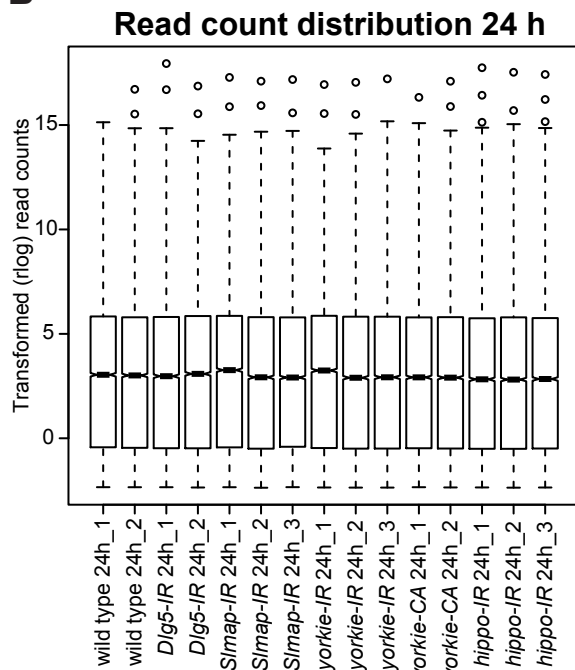
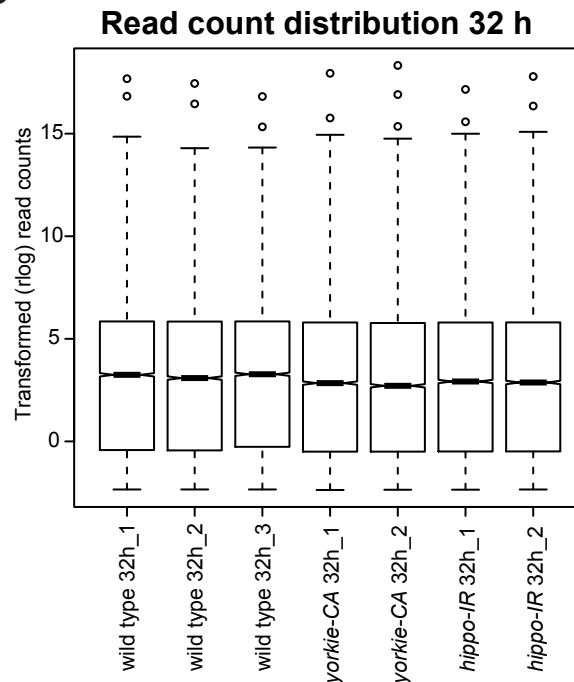
**B****C**

Figure 7 Supplement 1